Apertureless Scanning Near-Field Optical Microscope Probe for Transmission Mode Operation

Dissertation submitted to the faculty of Sciences of the University of Neuchâtel, in fulfillment of the requirements for the degree of *"Docteur ès Sciences"*

by

Laure Aeschimann

Dipl. Ing. Phys. EPFL

Institute of Microtechnology
University of Neuchâtel
Rue Jaquet-Droz 1, CH-2007 Neuchâtel
Switzerland

July 2004

IMPRIMATUR POUR LA THESE

Apertureless Scanning Near-Field Optical Microscope Probe for Transmission Mode Operation

Mme Laure AESCHIMANN

UNIVERSITE DE NEUCHATEL

FACULTE DES SCIENCES

La Faculté des sciences de l'Université de Neuchâtel, sur le rapport des membres du jury

MM. U. Staufer (directeur de thèse), N.F. de Rooij, O. Martin (EPF Lausanne) et A.F. Meixner (Siegen D)

autorise l'impression de la présente thèse.

Neuchâtel, le 27 août 2004

La doyenne:

Prof. M. Rahier

Abstract

In addition to providing optical imaging at the subwavelength scale with high resolution topography, a main advantage of scanning near-field optical microscopy (SNOM) is its capability to benefit from the various contrast mechanisms of conventional optical microscopy. However, broad application of SNOM suffers from the difficulty of producing inexpensive probes of high reproducible quality. The motivation of this thesis is the development and the characterization of a microfabricated probe which is well suited for mass production.

The developed probe comprises a 11μm high $Si0_2$ tip integrated on a silicon cantilever, which permits its operation in all modes of force microscopy. Underneath the tip, a hole is etched in the cantilever for light injection or detection from the backside. The microfabrication of the probes has been adapted to meet industrial standards. Despite the fact that the tips are entirely coated with an opaque metal layer, for instance aluminum, high light throughput can be observed. Moreover, high optical resolution imaging below 100nm could be demonstrated with such probes. Theoretical modelling and several far-field and near-field experiments have been performed in order to investigate the mechanism of light transmission through the probes as well as the physical process of image formation.

Theoretical calculations and experimental results suggest that a field enhancement occurs at the tip apex due to lightning rod effect. No plasmon effects are expected and indeed observed. Moreover, sharper tips show

higher transmittance, what is also verified by the theoretical model. Further, very pronounced emission characteristics of the probes are shown as function of the considered polarization state. The theoretical model predicts that two modes propagate in the probe. The radially polarized mode leads to a subwavelength field confinement at the tip apex whereas the linearly polarized mode induces a light leakage at the tip flanks. Experimentally, when coupling linearly polarized laser light into the tip, characteristic far-field emission patterns are observed, when polarizers positioned in front of the cantilever entrance and behind the tip apex, are either parallel or crossed by 90 degrees. We assume that these experimentally observed polarization states can be understood in terms of the modes propagating through the tip. If so, both modes are excited at the tip entrance or exit even if linearly polarized light is injected. Based on this interpretation, when a polarizer is used in order to block the light leaking at the tip walls, a better image quality is expected and indeed observed.

It is important to notice that non repeatable results have been obtained with reproducibly fabricated probes. The different probe characterizations have shown that a large number of different parameters, like light coupling aspects or the metal coating roughness, must be taken into consideration when experimenting with the probes and that the interpretation of the obtained results is very complex.

Résumé

La résolution en microscopie classique est limitée par la diffraction de la lumière. Grâce à la microscopie optique en champ proche (SNOM), il est possible de dépasser cette barrière. De plus, cette technique permet d'obtenir conjointement à l'image optique, une image de la topographie de la surface de l'échantillon, de façon similaire à celle obtenue en microscopie à force atomique. Une application à large échelle de la microscopie optique en champ proche est toutefois freinée par la difficulté de produire des sondes reproductibles, bon marché et de haute qualité. La motivation de cette thèse est le développement d'une telle sonde adaptée à la production de masse.

La sonde développée est constituée d'une pointe transparente haute de 11μm fabriquée en $Si0_2$ et intégrée sur un levier en silicium. Cette sonde est adaptée à tous les modes de fonctionnement connus en microscopie à force atomique. Une ouverture dans le levier, située juste au-dessous de la pointe, permet le couplage ou la détection de la lumière. Le procédé de microfabrication des sondes a été adapté aux normes industrielles. Une forte transmission de lumière peut être mesurée à travers les pointes, bien que celles-ci soient entièrement recouvertes d'une couche opaque de métal, comme par exemple de l'aluminium. De plus, il a été démontré que ces sondes permettent d'atteindre une résolution optique inférieure à 100nm. Afin d'étudier les mécanismes physiques permettant à la lumière de se propager et d'être transmise à travers de telles sondes, des modélisations théoriques ainsi que différentes expériences ont été effectuées.

La théorie ainsi que les résultats expérimentaux obtenus suggèrent qu'un effet de champ apparaît au bout de la pointe. Aucune excitation de plasmons dans la couche métallique n'est observée. En outre, une plus forte transmission est mesurée à travers des pointes dont l'angle d'ouverture est plus faible, ce qui a été également confirmé par le modèle théorique. Une émission de lumière très caractéristique est observée en fonction de l'état de polarisation. Le modèle théorique prédit que deux modes du champ électromagnétique se propagent dans la pointe. Le mode polarisé radialement crée un champ très confiné au bout de la pointe, alors que le mode polarisé linéairement produit une fuite de lumière sur les flancs de la pointe. Les propriétés de polarisation de la lumière émise par la pointe ont été étudiées lorsqu'un faisceau de lumière polarisé linéairement est couplé dans la pointe et qu'un polariseur est placé devant le détecteur. En effet, dans le cas d'un polariseur placé parallèlement ou perpendiculairement à la polarisation d'entrée, deux émissions très caractéristiques sont observées. Nous pensons que ces états de polarisation observés peuvent être interprétés en termes de modes se propageant dans la pointe. Dans ce cas, même si un faisceau de lumière polarisée linéairement est couplé dans la pointe, les deux modes sont excités. En se basant sur cette interprétation, une meilleure qualité d'image est attendue et effectivement observée lorsqu'un polariseur est utilisé lors de la mesure afin de bloquer l'émission de lumière sur les flancs de la pointe.

Il est important de signaler que des résultats non reproductibles ont été obtenus avec des sondes fabriquées de façon reproductible. Les différentes expériences de caractérisation des sondes ont démontré qu'un grand nombre de paramètres, tels que le couplage de la lumière ou la rugosité du métal doit être pris en considération lors de l'expérimentation avec les sondes. Par conséquent, l'interprétation des résultats obtenus est extrêmement complexe.

Contents

List of Figures

Chapter 1

Introduction

Optical microscopy provides a wealth of information and allows one to investigate samples at ambient conditions. Unfortunately, it is not possible to improve conventional optical imaging techniques because of their limited resolution by diffraction to about half the wavelength of the light. By reducing the size of the detector however and by moving it into the near-field, i. e. very close to the sample surface, the optical resolution can be significantly increased.

The possibility to mechanically control objects at distances of nanometers or even Ångströms has been enabled by the invention of scanning probe technology. The basic principle of scanning probe microscopy (SPM) is the *probing* of a sample surface with a sharp tip mounted on a soft cantilever beam. SPM allows the characterization of surface topography with a resolution down to the atomic scale.

Thus, the combination of the power of optical microscopy with the potential of scanning probe technology gives us the possibility to have an *eye* for the nanoworld.

In a conventional configuration of scanning near-field optical microscopy (SNOM), a sub-wavelength sized source or detector is used to probe the sample. The major reason why SNOM is not a routinely used tool, is the absence of high-quality, reproducible and low-cost near-field probes. One

promising way to manufacture such SNOM sensors is to use well-established microfabrication techniques.

This chapter introduces the working principles of atomic force microscopy (AFM) and scanning near-field optical microscopy (SNOM) and points the interested reader to more fundamental publications. One goal of the present thesis is to combine these two microscopy techniques, in particular to batch fabricate combined AFM and SNOM probes in a reproducible way.

1.1 Atomic Force Microscopy (AFM)

The ability of the atomic force microscope (AFM) to create three-dimensional images with resolution down to the nanometer and Ångström scales has made it an essential tool for imaging surfaces in applications ranging from semiconductor processing to cell biology. In addition to topographical imaging, the AFM can also probe nanomechanical and other fundamental properties of sample surfaces, including their local adhesive or elastic properties.

In this section, the basics of AFM operation will be described briefly.

1.1.1 Principles of AFM

Atomic force microscopy, invented in 1985 by Binnig, Quate and Gerber [1], belongs to the group of scanning probe microscopy (SPM), a family of microscopes where a sharp probe is scanned across a surface and some probe-sample interactions are monitored.

The key element of the AFM is the microscopic force sensor consisting of a cantilever with an integrated tip. The cantilever is usually formed by one or more beams of silicon or silicon nitride 100 to 500μm long and about 0.5 to 5μm thick. Mounted on the end of the cantilever is a sharp tip that is used to probe the sample surface. The forces acting between the tip and the sample cause the cantilever to bend or deflect. A detector measures the cantilever deflection as the tip is scanned over the sample surface by a piezoelectric scanner. A feedback control loop maintains a constant deflection between the cantilever and the sample by vertically moving the scanner

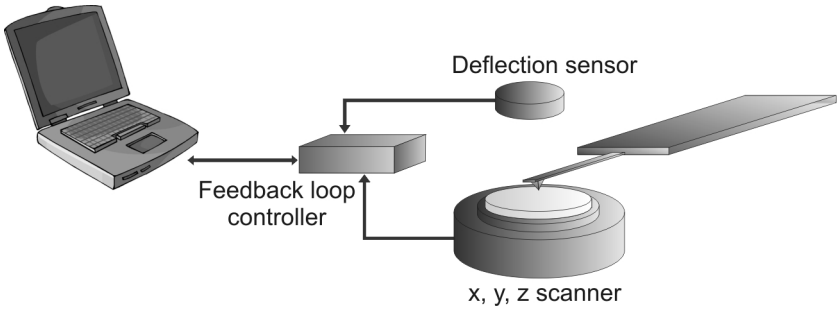

Figure 1.1: Schematic of an AFM setup. A force sensor probes the surface and a feedback control permits to drive the x, y, z piezo-actuators.

and regulating the tip-sample distance. The precision motion of the scanner is monitored to generate the topographic images and force measurements (Fig. 1.1).

Forces of different nature contribute to the deflection of the AFM cantilever as depicted in Fig. 1.2. When the tip is in contact with the sample, the interatomic force between the probe and the sample is repulsive. If the distance is increased, longer-range attractive forces, like Van der Waals, capillary, magnetic or electrostatic forces cause the cantilever to deflect.

1.1.2 Operation modes

AFM can be operated in different modes of operation, basically depending on the working distance between the tip and the sample. Most commonly, three modes are used: contact, non-contact and intermittant contact modes.

In contact mode, the tip is in "physical contact" or in very close proximity with the sample. The force applied on the tip is measured directly by the deflection of the cantilever. The force is kept constant by maintaining the cantilever deflection constant with a feedback loop. A low spring constant (typically 0.01N/m to 1N/m) of the cantilever is needed to avoid big forces, which may cause damage to the tip or to the sample.

In non-contact mode, the tip is maintained at a short distance from the sample, usually around 10nm, and vibrates near its resonance frequency.

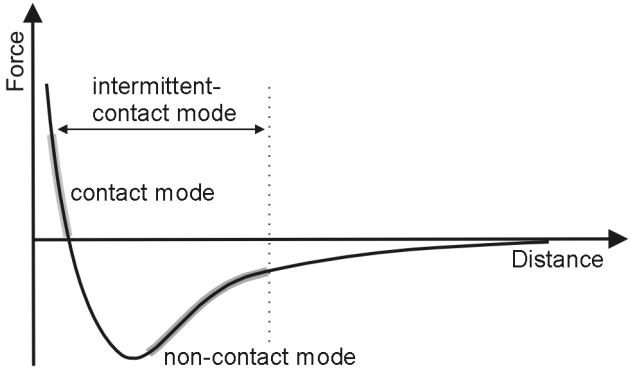

Figure 1.2: Schematic of force versus probe to sample distance. Long-range forces detected in non-contact mode AFM are in the regime of attractive forces. In contact mode the acting forces are repulsive.

The gradient of the force acting between the sample and the tip acts to change the cantilever vibration. This change is then detected by measuring either the amplitude, the phase or the frequency shift of the oscillation. Cantilevers used for non-contact AFM must be stiffer (typical spring constant of 20-100N/m) than those used for contact mode imaging, because soft cantilevers can be pulled into contact with the sample surface.

In an intermediate mode, known as intermittent-contact mode, the cantilever is oscillated near its resonance frequency and brought in very close proximity to the sample, so that it just hits the sample when it is at the bottom of its travel. Because the contact with the sample is only intermittent, the probe exerts negligible frictional forces on the sample. This imaging mode permits imaging delicate soft samples with less damage than contact mode, but with higher lateral resolution than non-contact mode.

1.1.3 Cantilever deflection detection techniques

As described above, the cantilever is deflected by a force. Several methods can be used to sense this deflection and some of these are presented in this paragraph.

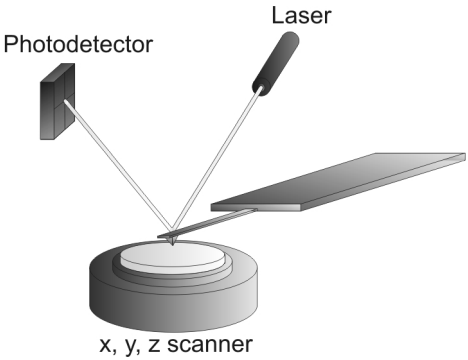

Figure 1.3: In the beam deflection technique a laser beam is focused on the cantilever back and directed on a position-sensitive photodiode.

The first method employed in the very first AFM set-ups was based on electron tunneling between a tunneling tip and the backside of the cantilever [1].

However, the beam deflection method is currently the mostly used technique for monitoring the displacement of the cantilever in AFM systems [2]. In this case, a laser beam is focused on the back of the cantilever and the reflected beam is sent to a position-sensitive photodiode (usually a four quadrant photodiode). During operation of the AFM, the difference in the intensity of the signal produced by each quadrant measures the deflection of the cantilever as depicted in Fig. 1.3. This very simple technique is commonly used in commercial systems and offers a very good sensitivity.

Integrating sensors directly in the AFM probe leads to very compact systems. One example is to sense the cantilever deflection with integrated piezoresistors. The strong dependence of the resistivity of silicon on applied stress is exploited in this case to detect the cantilever deflection [3]. Such detection elements have been successfully used for parallel imaging [4].

1.2 Scanning Near-field Optical Microscopy (SNOM)

The SNOM is a combination of a light microscope and a SPM. Although the idea on which SNOM is based goes back to 1928 [5], it could be demonstrated with visible light only in 1984 [6]. There is considerable interest in SNOM, but to date it has not evolved into a widely established imaging technique, since the quality of the probes is still low and especially difficult to fabricate in a reproducible way.

The following section gives a short introduction to near-field optics and shows the working principle of SNOM.

1.2.1 Optical near-field

The operation of conventional optical imaging systems suffers from the diffraction barrier, which limits the optical resolution. The theoretical limit of resolution, also known as the Rayleigh criterion, is given by the minimum distance *d* by which two points must be separated to be distinguishable. It is given by the relation

$$d = \frac{0.61\lambda}{NA} \tag{1.1}$$

where λ is the optical wavelength and NA the numerical aperture of the imaging lens. As might be expected, higher numerical aperture lenses can resolve points that are closer together. For visible light the resolution is limited to 0.2-0.4μm.

It is difficult to improve the definition of an optical system by scaling down the wavelength even to the near ultraviolet, because of the lack of suitable light sources and lens materials. To further reduce the wavelength, electrons can be used.

But, this diffraction barrier is not fundamental. This limit arises from the assumption that the detection system is placed typically many wavelengths away from the sample of interest. The resolution can be improved by reducing the size of the detector, and by decreasing the distance between the sample and the detector, i.e. moving the detector into the near-field.

One way to describe the optical near-field consists of analyzing the diffracted field by the Fourier theory [7, 8]. This approach leads to an interpretation in terms of propagating and evanescent waves.

Consider a plane wave $\vec{E}$ incident on a transverse plane (x,y), propagating in the positive z direction. The electric field $\vec{E}(x,y,0)$ across that plane (z=0) is considered to be known. The goal is to calculate the resulting field $\vec{E}(x,y,z)$ that appears in a parallel plane at a distance z of the first plane.

To solve this problem, consider the 2-dimensional Fourier transform of the electric field in z=0

$$\vec{E}(f_x, f_y; 0) = \int_{-\infty}^{\infty}\int_{-\infty}^{\infty} \vec{E}(x,y,0)e^{-2\pi i(f_x x + f_y y)}dxdy \tag{1.2}$$

where f_x and f_y are the spatial frequencies of the plane structures, which can in general take all values from 0 to ∞.

Thus, $\vec{E}(x,y,0)$ can be written as an inverse Fourier transform of its spectrum

$$\vec{E}(x,y,0) = \int_{-\infty}^{\infty}\int_{-\infty}^{\infty} \vec{E}(f_x, f_y; 0)e^{2\pi i(f_x x + f_y y)}d\,f_x d\,f_y \tag{1.3}$$

Similarly, the electric field in z>0 is given by

$$\vec{E}(x,y,z) = \int_{-\infty}^{\infty}\int_{-\infty}^{\infty} \vec{E}(f_x, f_y; z)e^{2\pi i(f_x x + f_y y)}d\,f_x d\,f_y \tag{1.4}$$

In homogeneous, isotropic and linear media the $\vec{E}$ field has to satisfy the Helmholtz equation $\nabla^2\vec{E} + k^2\vec{E} = 0$. Direct application of this requirement to equation 1.4 shows a solution that can be written in the form

$$\vec{E}(f_x, f_y, z) = \vec{E}(f_x, f_y; 0)e^{2\pi i\sqrt{\frac{1}{\lambda^2} - f_x^2 - f_y^2}z} \tag{1.5}$$

where $k = 2\pi/\lambda$ is the magnitude of the wave vector $\vec{k}$ of the propagating wave. Equation 1.5 in 1.4 gives the value for the electric field in z>0

$$\vec{E}(x,y,z) = \int_{-\infty}^{\infty}\int_{-\infty}^{\infty} \vec{E}(f_x, f_y; 0) e^{2\pi i (f_x x + f_y y + \sqrt{\frac{1}{\lambda^2} - f_x^2 - f_y^2} z)} d f_x d f_y \qquad (1.6)$$

Equation 1.5 is an oscillating function for $f_x^2 + f_y^2 < \frac{1}{\lambda^2}$ and an exponentially decreasing function for $f_x^2 + f_y^2 > \frac{1}{\lambda^2}$. Thus, if the image plane is sufficiently separated from the source plane, the contribution of the decreasing parts is zero. There is hence a loss of information on the way of propagation.

In the first case ($f_x^2 + f_y^2 < \frac{1}{\lambda^2}$) the spatial frequencies correspond to structures whose dimensions are bigger than λ. The exponent of equation 1.5 is imaginary and the corresponding waves propagate from the object plane toward the detector in the far-field. These propagating waves transmit the low spatial frequencies of the object, containing information about its most significant characteristics.

In the second case ($f_x^2 + f_y^2 > \frac{1}{\lambda^2}$) the spatial frequencies correspond to structures whose characteristic dimensions are smaller than the wavelength. The exponent of equation 1.5 is negative, e.g. the waves are exponentially attenuated in z-direction. They correspond to *evanescent* waves. These evanescent waves are related to the high spatial frequencies of the object of interest, which contain information about its smallest details.

Obviously, the improvement of spatial resolution in optical microscopy demands the detection of the high-frequency spatial components. By approaching a probe in close proximity to the object's surface, evanescent waves can be transformed into propagating ones and thereby recover information that would otherwise be lost.

This is exactly what near-field optics deal with. Different schemes of probes were invented to convert the evanescent fields into propagating ones that can easily be detected by conventional far-field optics.

1.2.2 Principles of SNOM

The concept of scanning near-field optical microscopy was proposed in 1928 by Synge [5]. The idea is to illuminate the sample through a tiny aperture in

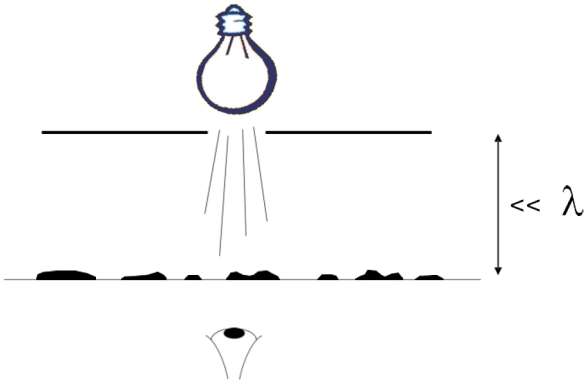

Figure 1.4: The generic SNOM set-up proposed by Synge [5]. A subwavelength sized light source is raster-scanned across the sample surface at a distance much smaller than the wavelength of the light.

an opaque screen and observe the transmitted light as depicted in Fig. 1.4. The aperture has to be placed in optical near-field distance to the sample. The image can be reconstructed by scanning the aperture over the sample surface. The resolution is, then, essentially given by the diameter of the aperture. This imaging scheme can also be inverted and the aperture plays in that case the role of a local detector.

The difficulty of approaching the sample with a planar screen, is circumvented by the fabrication of a subwavelength sized optical aperture placed at the apex of a sharply pointed tip. By implementing a feedback loop the distance between the tip and the sample surface can be regulated.

Different experimental configurations are able to generate optical images with nanometer resolution. Some of those are described briefly in the next few paragraphs. A good overview of these different techniques can be found in reference [9].

Illumination mode: This mode of operation is the most commonly used SNOM imaging mode. The aperture is used as a localized light source, which illuminates the sample (Fig. 1.5a)). The light emitted at the tip apex is transmitted through the sample and is detected in the far-field. The image

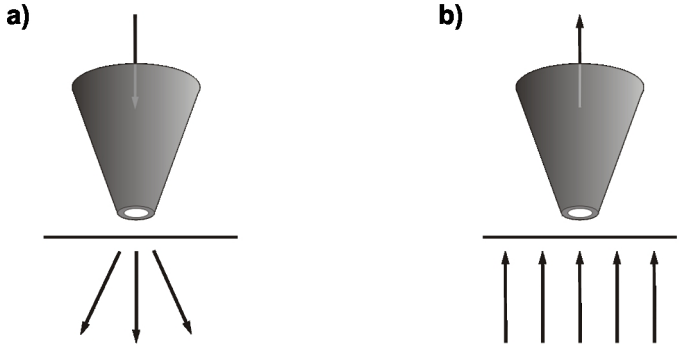

Figure 1.5: In illumination mode (a) the probe illuminates the sample and the light is collected in the far-field. In the collection scheme (b) the probe collects the light coming through the sample, which is illuminated from the far-field.

is reconstructed point by point while the tip is scanned over the sample.

Collection mode: In collection mode, the tip acts like a local probe to collect the light coming through the sample as depicted in Fig. 1.5b). The sample is illuminated globally from the far-field.

Apertureless SNOM: An alternative to the aperture probe in SNOM, is a scattering tip operated in the so-called apertureless SNOM configuration [10, 11, 12, 13]. In apertureless SNOM, a sharp probe illuminated by external (far-field) illumination scatters the electromagnetic field locally at its apex and, therefore, acts like a local source (Fig. 1.6a)). Therefore, the relevant near-field optical signal has to be extracted from a large background of unwanted stray light from the sample surface. A method to decrease the stray light is a lock-in detection technique. The tip is vibrated at a certain frequency and the detected signal is demodulated with a lock-in detection scheme. Evanescent illumination using total internal reflection is an alternative method used to reduce the unwanted scattered light (Fig. 1.6b)). The evanescent field generated over the sample surface is scattered by the probe and the scattered light is collected by external optics.

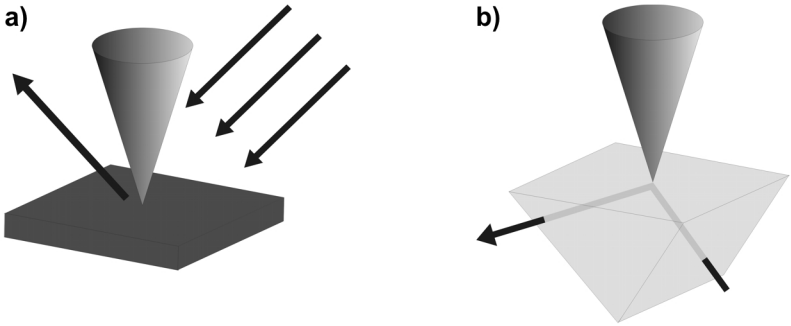

Figure 1.6: In one configuration of apertureless SNOM (a) the sample is illuminated by far-field illumination. The light that is scattered by the oscillating tip and the sample, is collected using a lock-in detection scheme. In a second configuration (b), an evanescent field is generated over the sample surface by total internal reflection. This field is scattered by the probe and detected with external optics.

A variation of the apertureless SNOM experiment is the combination of SNOM with Raman spectroscopy, providing a promising tool for analyzing the molecular composition of complex materials. A major drawback of Raman methods is the low scattering cross-section which makes the detection of single scatterer impossible. However, by using surface enhanced Raman scattering (SERS) this difficulty can be overcome. In this technique an amplification of the Raman signals is induced by metallic nanoparticles. Huge enhancement factors of up to 10^{15} have been reported, allowing to perform Raman spectroscopy even at the single molecule level [14, 15]. Raster scanning the sample with a metal tip allows one to combine topography and Raman imaging with nanometer resolution. Raman enhancement using metal tips has been successfully demonstrated, for instance on single molecules [16] or single-walled carbon nanotubes [17].

1.2.3 Fiber based SNOM probes

In many of today's near-field optical microscopes specially processed optical fibers are used as probes. For this purpose, a glass fiber is tapered into a

tip, metallized and a subwavelength aperture is patterned at its apex.

Two principle methods have been proposed to shape optical fibers into tips. In the first technique, the heating and pulling method, the fiber is locally heated and simultaneously stretched [18]. During this procedure the fiber gets thinner until it breaks. The broken fiber ends show a tip shape with a flat end at its apexes. The second method is based on etching the fiber in an aqueous solution of hydrofluoric acid (HF). Chemical etching provides fiber probes with larger cone angles and higher optical throughput [19, 20].

After shaping into a tip, the fiber is covered with an opaque metal coating and a small aperture has to be structured at the tip apex. Commonly, aluminum is chosen as coating material because of its small skin depth (12.7nm at λ=500nm). In order to create an aperture at the tip apex, the metal evaporation is done while rotating the fiber under an angle such that the apex of the tip stays uncovered [21]. The resulting aperture shapes are often irregular and their size not very reproducible. Another way to create apertures is to pattern the tip apex by focused-ion-beam (FIB) milling [22]. The size and the shape of the opening can be well defined and controlled, but the technique is expensive. An aperture formation method based on local etching by a solid electrolyte also gives high aperture definition, but an elaborated set-up is needed [23].

In the case of fiber based SNOM probes, the tip-sample distance regulation is achieved by the so-called shear-force mode [24, 25]. The fiber is placed vertically in respect to the sample surface and the end of the fiber is oscillated laterally near its resonance frequency. Due to forces acting between the tip and the sample, the oscillation is damped when the tip approaches the surface. The change in the vibration amplitude or frequency is monitored and used as feedback signal to control the tip-sample separation.

Major drawbacks of these probes are their fragility and the damping of the shear-force detection scheme that is still little understood. In particular, the high longitudinal stiffness of the fiber brings with it the risk of damage to both the sample and the probe during unwanted contact. AFM distance control can be applied for special bent fiber probes [26]. But, these probes are difficult to fabricate and are very stiff, what makes them unusable for some applications. Moreover, all described fabrication methods are serial

processes. This means that no large number of probes can be produced at the same time with reproducible properties.

1.2.4 Cantilever based SNOM probes

Using micromachining, some of the above mentioned problems for SNOM probe fabrication can be avoided and the production of the resulting probes is potentially cheap and highly reproducible.

Furthermore, integrating a SNOM tip into a AFM cantilever enables imaging of the sample in all modes of force microscopy and, thus, provides a good method of probe-to-sample distance control. Moreover, microfabrication opens the possibility to add deflection sensors or actuators into the cantilever, leading potentially to parallel imaging.

Different approaches of cantilever based SNOM probes have been presented. Silicon nitride probes produced by molding technique [27] or silicon nitride tips integrated on a cantilever with an optical waveguide structure [28] have been fabricated and used for imaging. Batch fabrication of hollow metal tips with apertures <100nm mounted on silicon cantilevers have been proposed by Mihalcea *et al.* [29].

In the above presented approaches of cantilevered SNOM probes, the most demanding aspect is the structuring of a small aperture into the opaque metal film at the tip apex. The aperture is usually introduced during the initial fabrication process. A selective reactive ion etching method for sub-100nm aperture formation based on tip effects has been proposed by Schürmann *et al.* [30]. Another process to fabricate apertures of high quality at the apex of aluminum-coated silicon-nitride tips by a self-terminated corrosion process has been presented [31].

An innovative design of batch fabricated aluminum coated solid quartz tips integrated on silicon cantilevers has been presented by Schürmann *et al.* [32]. In the case of fully aluminum coated tips, imaging of single molecules with a lateral optical resolution of 32nm has been shown [33].

1.3 Summary and conclusions

The key element of SNOM is the near-field optical probe that rasters the object field in the evanescent region. Among the various concepts that have been adopted to produce near-field optical probes, a SNOM tip mounted at the end of an AFM cantilever is an ideal probe for near-field optical microscopy. The major difficulty in fabricating such probes, is the structuring of a small aperture at the tip apex.

The high transmission through fully metal coated quartz tips observed by Schürmann *et al.* [32] is very promising. In fact, such probes permit high optical resolution avoiding the problem of aperture manufacturing. Further, the granular nature of the metallic coatings surrounding apertures often results in small random metal grains at the tip apex. It is shown that this metal roughness has a large impact on the emission characteristics of the near-field probes [34]. This can also lead to a shift between the optical and topographic signals, and frequently prevents the tip aperture from sufficiently approaching the surface of the sample. This problem is of course weakened by using tips without an aperture.

Bibliography

[1] G. Binnig, C. F. Quate, C. Gerber. *Atomic force microscope*. Phys. Rev. Lett. **56**, 930 (1986).

[2] G. Meyer, N. M. Amer. *Novel optical approach to atomic force microscopy*. Appl. Phys. Lett. **53**, 1045 (1988).

[3] M. Tortonese, R. C. Barrett, C. F. Quate. *Atomic resolution with an atomic force microscope using piezoresistive detection*. Appl. Phys. Lett. **62**, 834 (1993).

[4] S. C. Minne, S. R. Manalis, C. F. Quate. *Parallel atomic force microscopy using cantilevers with integrated piezoresistive sensors and integrated piezoelectric actuators*. Appl. Phys. Lett. **67**, 3918 (1995).

[5] E. H. Synge. *A suggested method for extending microscopic resolution into the ultra-microscopic region*. Phil. Mag. and J. of Science **6**, 356 (1928).

[6] D. W. Pohl, W. Denk, M. Lanz. *Optical stethoscopy: Image recording with resolution lamda/20*. Appl. Phys. Lett. **44**, 651 (1984).

[7] J. W. Goodman. *Introduction to Fourier optics*. McGraw-Hill, San Fransisco, (1968).

[8] G. A. Massey. *Microscopy and pattern generation with scanned evanescent waves*. Appl. Opt. **23**, 658 (1984).

[9] H. Heinzelmann, D. W. Pohl. *Scanning near-field optical microscopy*. Appl. Phys. A **59**, 89 (1994).

[10] U. C. Fischer, D. W. Pohl. *Observation of single-particle plasmons by near-field optical microscopy*. Phys. Rev. Lett. **62**, 458 (1989).

[11] D. Courjon, J.-M. Vigoureux, M. Spajer, K. Sarayeddine, S. Leblanc. *External and internal reflection near-field microscopy: experiments and results*. Appl. Opt. **29**, 3734 (1990).

[12] F. Zenhausern, Y. Martin, H. K. Wickramasinghe. *Scanning interferometric apertureless microscopy: Optical imaging at 10 Angstrom resolution*. Science **269**, 1083 (1995).

[13] Y. Inouye, S. Kawata. *Reflection-mode near-field optical microscope with a metallic probe tip for observing fine structures in semiconductor materials*. Opt. Comm. **134**, 31 (1997).

[14] K. Kneipp, Y. Wang, H. Kneipp, L. T. Perelman, I. Itzkan, R. R. Dasari, M. S. Feld. *Single molecule detection using surface-enhanced raman scattering (SERS)*. Phys. Rev. Lett. **78**, 1667 (1997).

[15] S. Nie, S. R. Emory. *Probing single molecules and single nanoparticles by surface-enhanced raman scattering*. Science **275**, 1102 (1997).

[16] R. M. Stöckle, Y. D. Suh, V. Deckert, R. Zenobi. *Nanoscale chemical analysis by tip-enhanced Raman spectroscopy*. Chem. Phys. Lett. **318**, 131 (2000).

[17] A. Hartschuh, N. Anderson, L. Novotny. *Near-field Raman spectroscopy using a sharp metal tip*. J. Microscopy **210**, 234 (2003).

[18] G. A. Valaskovic, M. Holton, G. H. Morrison. *Parameter control, characterization, and optimization in the fabrication of optical fiber near-field probes*. Appl. Opt. **34**, 1215 (1995).

[19] A. Sayah, C. Philipona, P. Lambelet, M. Pfeffer, F. Marquis-Weible. *Fiber tips for scanning near-field optical microscopy fabricated by normal and reverse etching*. Ultramicroscopy **71**, 59 (1998).

[20] R. Stöckle, C. Fokas, V. Deckert, R. Zenobi, B. Sick, B. Hecht, U. P. Wild. *High-quality near-field optical probes by tube etching*. Appl. Phys. Lett. **75**, 160 (1999).

[21] E. Betzig, J. K. Trautman, T. D. Harris, J. S. Weiner, R. L. Kostelak. *Breaking the diffraction barrier: Optical microscopy on a nanometer scale*. Science **251**, 1468 (1991).

[22] J. A. Veerman, A. M. Otter, L. Kuipers, N. F. van Hulst. *High definition aperture probes for near-field optical microscopy fabricated by focused ion beam milling*. Appl. Phys. Lett. **72**, 3115 (1998).

[23] A. Bouhelier, J. Toquant, H. Tamaru, H.-J. Güntherodt, D. W. Pohl, G. Schider. *Electrolytic formation of nanoaperture for scanning near-field optical microscopy*. Appl. Phys. Lett. **79**, 683 (2001).

[24] E. Betzig, P. L. Finn, J. S. Weiner. *Combined shear force and near-field scanning optical microscopy*. Appl. Phys. Lett. **60**, 2484 (1992).

[25] R. Toledo-Crow, P. C. Yang, Y. Chen, M. Vaez-Iravani. *Near-field differential scanning optical microscope with atomic force regulation*. Appl. Phys. Lett. **60**, 2957 (1992).

[26] H. Muramatsu, N. Chiba, K. Homma, K. Nakajima, S. Ohta, A. Kusumi, M. Fujihira. *Near-field optical microscopy in liquids*. Appl. Phys. Lett. **66**, 3245 (1995).

[27] M. Radmacher, P. E. Hillner, P. K. Hansma. *Scanning nearfield optical microscope using microfabricated probes*. Rev. Sci. Instrum. **65**, 2737 (1994).

[28] M. Stopka, D. Drews, K. Mayr, M. Lacher, W. Ehrfeld, T. Kalkbrenner, M. Graf, V. Sandoghdar, J. Mlynek. *Multifunctional AFM/SNOM cantilever probes: fabrication and measurements*. Microelec. Eng. **53**, 183 (2000).

[29] C. Mihalcea, W. Scholz, S. Werner, S. Münster, E. Oesterschulze, R. Kassing. *Multipurpose sensor tips for scanning near-field microscopy*. Appl. Phys. Lett. **68**, 3531 (1996).

[30] G. Schürmann, P. F. Indermühle, U. Staufer, N. F. de Rooij. *Micromachined SPM probes with sub-100 nm features at tip apex*. Surface and Interface Analysis **27**, 299 (1999).

[31] D. Haefliger, A. Stemmer. *Subwavelength-sized aperture fabrication in aluminum by a self-terminated corrosion process in the evanescent field*. Appl. Phys. Lett. **80**, 3397 (2002).

[32] G. Schürmann, W. Noell, U. Staufer, N. F. de Rooij, R. Eckert, J. M. Freyland, H. Heinzelmann. *Fabrication and characterization of a silicon cantilever probe with an integrated quartz-glass (fused-silica) tip for scanning near-field optical microscopy*. Appl. Optics **40**, 5040 (2001).

[33] R. Eckert, J. M. Freyland, H. Gersen, H. Heinzelmann, G. Schürmann, W. Noell, U. Staufer, N. F. de Rooij. *Near-field fluorescence imaging with 32nm resolution based on microfabricated cantilevered probes*. Appl. Phys. Lett. **77**, 3695 (2000).

[34] O. J. F. Martin, M. Paulus. *Influence of metal roughness on the near-field generated by an aperture/apertureless probe*. J. Microscopy **205**, 147 (2002).

Chapter 2

Microfabrication

A combined AFM and SNOM probe design has been proposed by Schürmann *et al.* [1, 2]. The probe consists of a silicon AFM cantilever on which is integrated a 25μm high quartz tip. Underneath the tip, a hole in the cantilever allows the light to be focused into the tip from the backside. The tip is coated with aluminum to avoid the light from leaking out at the tip walls. The deflection of the cantilever can be measured with the beam deflection method. By imaging single molecules, an optical lateral resolution of about 32nm has been demonstrated with these probes [3].

The fabrication process of those SNOM probes contains many critical steps and some serial processing is needed [1, 2]. In particular, the integration of a quartz structure on a silicon wafer by bonding is very difficult. This arises from the fact that the expansion coefficients of quartz and silicon differ by nearly one order of magnitude ($5 \cdot 10^{-7}$ for quartz and $3 \cdot 10^{-6}$ for silicon). Thus, once a quartz structure is integrated on the silicon wafer, no further process step involving high temperatures can be used anymore. Otherwise, the stress between the quartz-silicon interface can lead to rupture of the structures. This point limits considerably the choice of materials that can be used during the processing (silicon nitrides, oxides and polysilicon are deposited at temperatures higher than 400°C). The bonding is a serial procedure, which is a further drawback of the fabrication process. Such fabrication steps have to be eliminated absolutely, in view of mass production

of the probes.

In this work, we reconsidered the fabrication sequence and propose a novel way to produce cantilever based SNOM probes with an integrated $Si0_2$ tip. The following micromachining techniques are used for this fabrication process:

- Standard photolithography
- Anisotropic wet etching of silicon in potassium hydroxide (KOH)
- Thermal growth of silicon dioxide
- Isotropic wet etching of silicon dioxide in buffered hydrofluoric acid (BHF)
- Low pressure chemical vapor deposition (LPCVD) of silicon nitride
- Dry etching of silicon nitride
- Metal evaporation

These microfabrication standard processing techniques are described elsewhere [4].

The detailed manufacturing steps of the cantilever based SNOM probes, as well as the fabrication results, are presented in the next paragraphs.

2.1 Requirements for the SNOM probes

As in all scanning probe microscopy techniques, the probe consisting of a cantilever and an integrated tip is the key element of the SNOM (Fig. 2.1).

The mechanical properties of the cantilever have to fulfill different conditions. The spring constant of the lever should be small for detecting weak forces. Moreover, a high resonance frequency of the cantilever permits to scan at fast speeds and to be less sensitive to external vibration.

In order to achieve such a low spring constant and a high resonance frequency, the mass and the dimensions of the cantilever should be small,

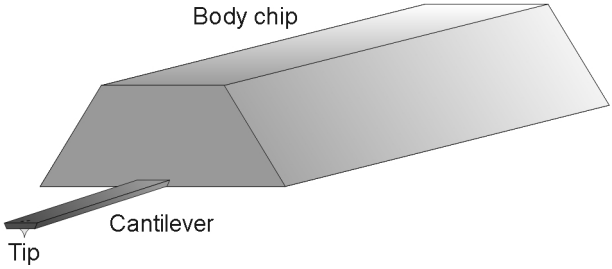

Figure 2.1: Schematic of a cantilever based SNOM probe, consisting of a body chip or handling piece and a cantilever on which is integrated a sharp tip. On the backside of the cantilever a hole allows optical access to the transparent tip.

which motivates applying micromachining technologies. Silicon turned out to be a well suited base material for such mechanical applications. Different etching techniques could be developed for integrating sharp tips on such cantilevers [5].

A particular requirement for SNOM cantilevers is that the backside of the tip has to be optically accessible. Hence, a hole must be processed into the cantilever, behind the tip. This opening has to be well centered with respect to the tip and has to show dimensions smaller than the tip base.

The tip also has geometric conditions to fulfill. It needs to be very sharp for a good lateral resolution in topography measurements. Further, the tip has to be transparent. Therefore, quartz ($Si0_2$) or fused silica is a good choice, because it is transparent to light from the visible to the ultra-violet range. It also doesn't show any internal fluorescence. The probe has finally to be covered with an opaque layer, e.g. a metal.

2.2 Silicon dioxide tips

$Si0_2$ tips can be fabricated from bulk material by wet or dry etching using a protection mask, for example silicon nitride. By correctly choosing the mask design, the desired tip shape can be achieved. Underetching is then responsible for the formation of the tip structure as depicted in Fig. 2.2 [6].

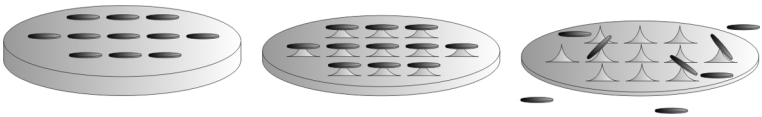

Figure 2.2: Schematic of tips realized by isotropic underetching. A mask material is deposited on the substrate and patterned (for example discs). The tips are formed during etching until the masks structures are completely underetched and fall off.

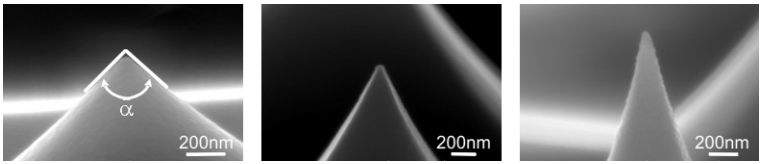

Figure 2.3: By isotropic underetching of quartz in BHF round tips can be manufactured. Overetched tips have larger cone opening angles α.

When using a disc shaped mask, isotropic etching will lead to circular tips. Because of imperfections during the lithography process, tips fabricated with square masks often terminate in a small knife-edge. Thus, disc shaped masks are usually preferred.

First, the fabrication of silicon dioxide tips is established. For this purpose, 250nm of LPCVD silicon nitride is deposited on a quartz wafer. The patterns (disc shaped, 13μm, 15μm and 16μm in diameter) for tip etching are structured by standard photolithography and transferred to the silicon nitride by dry etching. Isotropic wet etching in BHF is proceeded until the 16μm discs fall off. In this case, the resulting tips produced by the 15μm and 13μm structures are overetched. This leads to an enlarged cone opening angle of the tips. On Fig. 2.3 the three different cone opening angles α of 97˚, 55˚ and 33˚ are depicted.

2.3 SNOM probe fabrication sequence

The raw material for the fabrication of the probes consists of double side polished monocrystalline silicon wafers. A 12μm thick $Si0_2$ layer is grown on the wafer by thermal wet oxidation. Such wafers were originally developed for integrating optical compounds like planar waveguides on silicon structures. In our case, the bulk silicon will be used for manufacturing the body chip as well as the cantilevers, and the transparent tips will be fabricated from the thick oxide layer as explained in the following paragraphs.

2.3.1 Backside structuring and tip patterning (Fig. 2.4)

After cleaning, a 250nm thick layer of LPCVD silicon nitride is deposited on the wafer. Then, by photolithography the patterns for the structuration of the nitride on the backside of the wafer are defined. The dry etching of the silicon nitride is followed by the removal of 3μm of the underlying oxide by wet chemical etching in BHF. Then, by lithography the structures for the tip etching are patterned on the wafer front surface. Again, by dry etching, these patterns are transferred to the silicon nitride layer. These round nitride pads of 26μm diameter are used as masks for the tip formation.

In a next step, 9μm of $Si0_2$ is removed by wet etching in BHF. The tip masks will remain on the partially etched tip structures until the very end of the fabrication process. During this BHF etching, the oxide layer on the backside of the wafer is completely removed.

2.3.2 Cantilever definition and membrane etching (Fig. 2.5)

The oxide on the frontside of the wafer is then again patterned by photolithography for defining the cantilever structures. In this case, the photoresist has to be thick enough to cover entirely the partially etched tips. To achieve nicely shaped tips, it is important that the tip masks stay intact through the whole procedure. In order to define the cantilevers in the oxide layer, 700nm of oxide is removed by wet etching in BHF. Then, the photoresist is stripped and the wafer is cleaned.

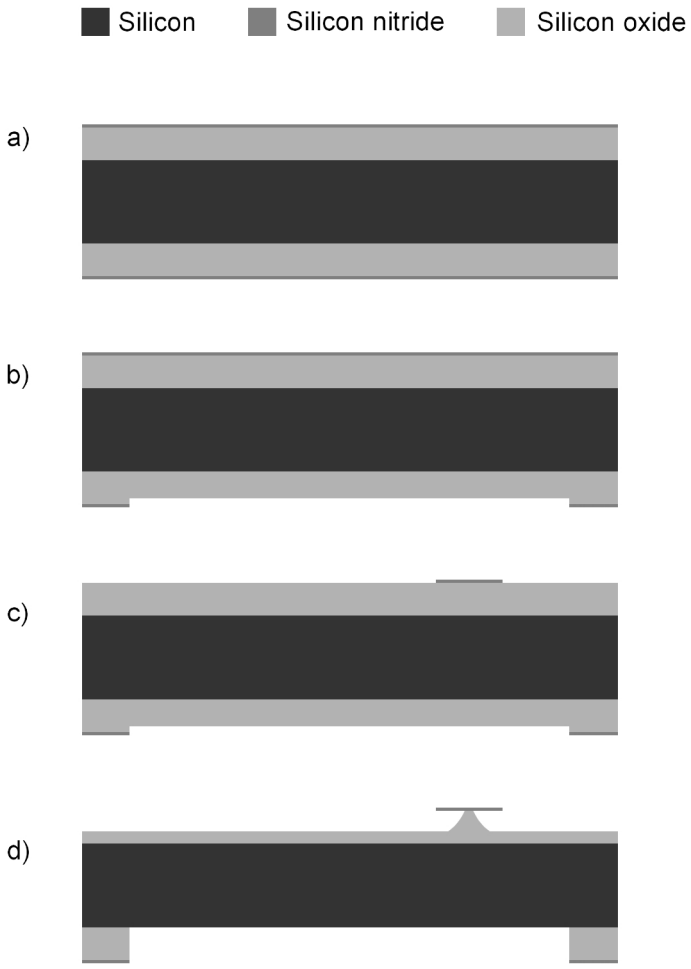

Figure 2.4: Schematic fabrication sequence (part 1): a) Silicon wafer with a 12μm thick thermal oxide layer and a 250nm thick LPCVD nitride layer. b) Backside structuring of the nitride and the oxide. c) Frontside patterning of the tip mask. d) Partial etching of the frontside oxide and total removal of the backside oxide.

The wafer is then etched anisotropically in KOH until a silicon membrane of about 5μm in thickness is formed. Notice that due do the total thickness variation of the wafer (TTV) and to non homogenous etching, the membrane thickness shows a certain dispersion across the wafer. For obtaining homogenous membranes and reproducible cantilevers across the wafer, it is necessary to choose wafers with very low TTV. Moreover, the KOH bath conditions as well as the etching time must be very carefully controlled. Several etching and thickness measurement steps are executed to produce the desired membrane thickness. During the KOH etching, the remaining oxide layer on the wafer front surface is used to protect the silicon. After the silicon etching is finished, this remaining frontside oxide is partially removed by BHF, such that the cantilevers are still defined by an oxide layer on the frontside of the wafer.

2.3.3 Hole structuring and cantilever releasing (Fig. 2.6)

After cleaning, a fresh thermal oxide layer of 250nm is grown on the wafer. This layer will be utilized as masking material for opening the hole in the backside of the cantilevers by means of KOH. The holes are patterned by photolithography on the backside of the wafer on the 5μm thick silicon membranes. For this purpose, a photoresist layer has to be deposited uniformly on the membranes in the deeply etched cavities. By spinning in a solvent atmosphere, a relatively low resist thickness variation can be achieved [7, 8]. But, in our case, spinning is hardly exploitable, because of the fragile tip masks on the wafer frontside and the thin silicon membranes that could be damaged. Another method to achieve a high homogeneity of the photoresist thickness across the membranes is spray coating. Such a technology has been developed by Electronics Vision Group, Austria. Investigations confirm the superior uniformity of photoresist coating by spray technology on wafers with high topography [9, 10].

First, the photoresist exposure was done with a standard aligner. In this case, diffraction seriously degrades the structure definition, because of the large gap between the mask and the substrate. The resulting large variations of the hole dimensions lead to a fabrication yield that is too low for

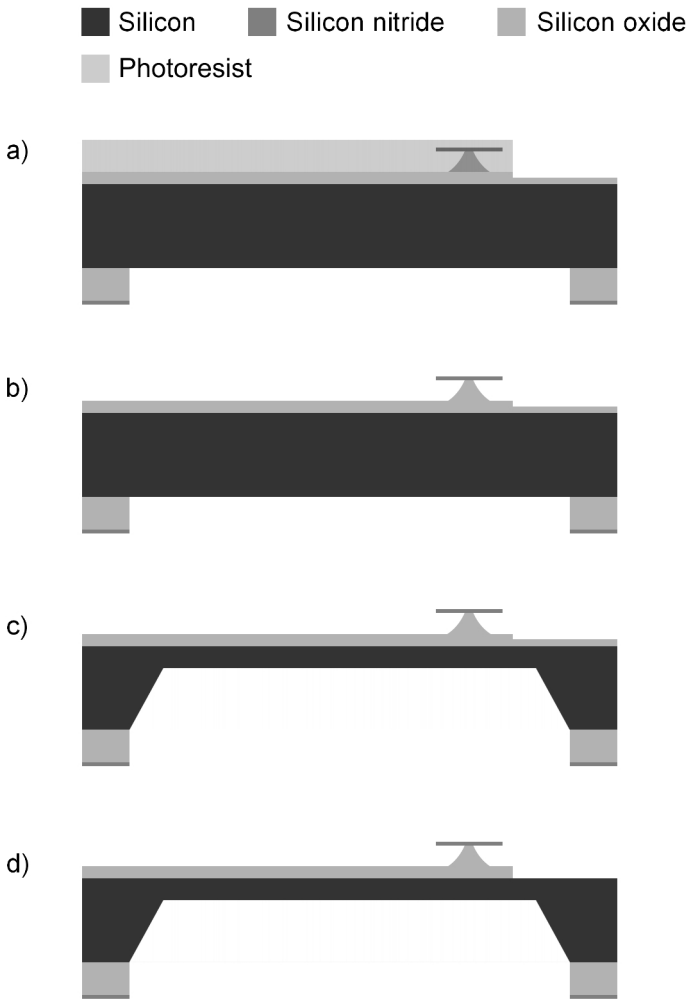

Figure 2.5: Schematic fabrication sequence (part 2): a) Photolithography and $Si0_2$ etching for the cantilever definition on the frontside. b) Photoresist stripping and wafer cleaning. c) Membrane formation through anisotropic wet etching of the silicon in KOH. d) Partial frontside $Si0_2$ removal. The cantilevers are still defined by a thin oxide layer.

mass production. This difficulty can be circumvented by using a projection aligner. In this case, the gap between the mask and the substrate can be large without affecting the pattern definition since the patterns are projected onto the substrate. The resulting hole structures show then the desired dimensions (round holes of 6μm in diameter).

Through wet etching in BHF the round shaped hole patterns are transferred into the 250nm thermal oxide layer. The following KOH attack permits to open the holes through the silicon membrane. Simultaneously, the cantilevers are released from the frontside during this etching step. After that, the oxide layer on the wafer backside has to be removed by wet etching in BHF.

2.3.4 Cantilever thinning and tip formation (Fig. 2.7)

In the next step, the silicon membrane has to be thinned down to 3μm to achieve the required mechanical properties of the cantilever. This thinning is performed by KOH etching of the backside of the wafer. The frontside is again protected by the remaining oxide layer. Notice, that during this etching, the opening in the membrane is exposed to the etchant and will enlarge. This post-etching doesn't affect the quality of the probes, since the opening near the tip base stays intact (Fig. 2.10 in paragraph 2.4).

In a final wet etching step in BHF, the tips are etched. Through several etching and measurement steps, the tip formation can be well controlled, until the tip masks fall off.

2.3.5 Metallization

Finally, the tips must be covered with an opaque metal coating. The selection of the metal as well as its deposited thickness on the tip is important. Because of its small skin depth, aluminum is often chosen as coating material. By evaporating nominally 100nm of aluminum on the wafer, a continuous layer of about 60nm thickness will cover the tip entirely, as transmission electron microscope images could show (see chapter 3, Fig. 3.1). The deposition is performed in the so-called "planetary" or "step coverage" mode. This method relies on rotating the wafers in planetary wafers holders so

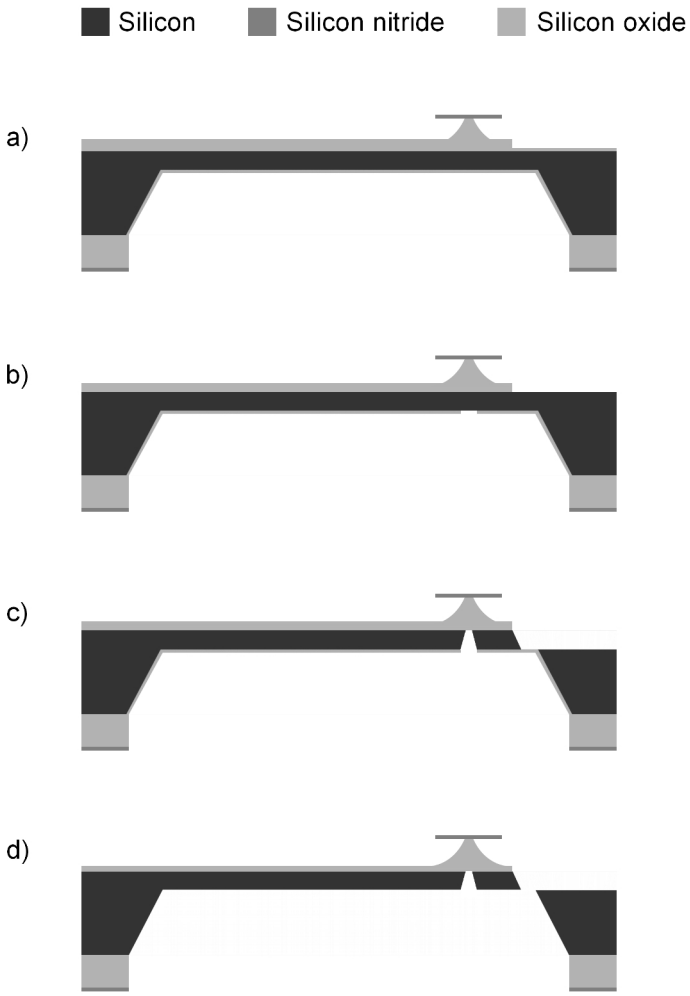

Figure 2.6: Schematic fabrication sequence (part 3): a) Thermal oxidation of the wafer (250nm thickness). b) Patterning of the hole structures from the backside by photolithography. c) KOH etching of the silicon leads to the opening formation on the backside and the cantilever releasing from the frontside. d) Removal of the remaining backside $Si0_2$ by wet etching in BHF.

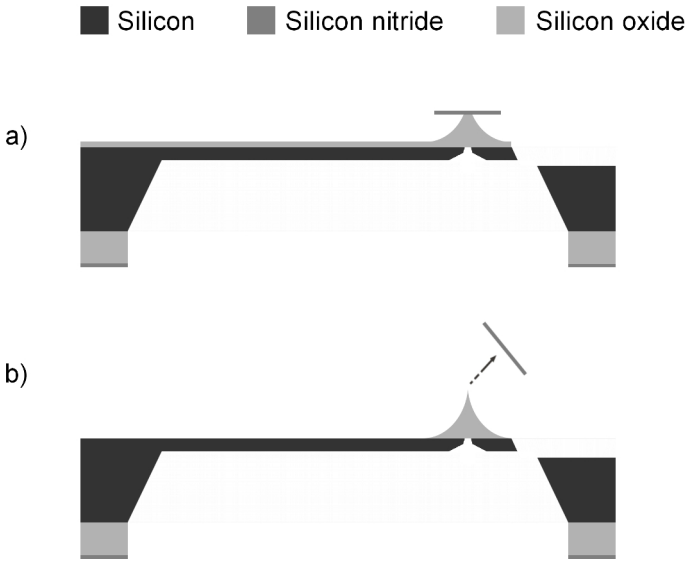

Figure 2.7: Schematic fabrication sequence (part 4): a) Thinning of the cantilever through KOH etching from the cantilever backside. b) BHF etching of the frontside $Si0_2$ leads to tip formation. The process is proceeded until the tip masks fall off.

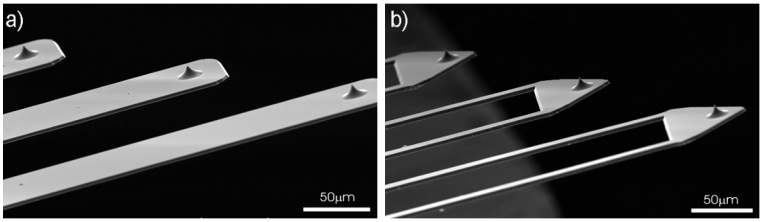

Figure 2.8: Scanning electron microscope (SEM) image of rectangular (a) and U-shaped (b) cantilevers with integrated quartz tip.

that the metal is evaporated under a constantly varying angle. It has to be noticed that prior to aluminum evaporation a 5nm thick layer of titanium is deposited as adhesion layer.

2.4 Fabrication results

The SNOM probes consist of a body chip on each side of which different cantilevers with tips are mounted. Rectangular and U-shaped cantilevers of variable lengths have been designed. The rectangular cantilevers are 80μm wide and 3μm thick. They are fabricated in three different lengths (Fig. 2.8a)) to be able to test their performance in contact or non-contact mode imaging. The cantilever lengths are 220μm, 320μm and 420μm, leading to calculated resonance frequencies of about respectively 86kHz, 40kHz and 23kHz and spring constants of respectively 8.6N/m, 2.8N/m and 1.2N/m. In view of applications in liquids, an U-shaped cantilever was also designed as shown in Fig. 2.8b). Such a shape permits the spring constant of the lever to be reduced and the liquid between the cantilever and the sample would be less compressed. Although, these probes are not further studied in this work, they show an interesting potential for applications in biology.

The tips have a round base shape and are about 11μm high as shown in Fig. 2.9.

As mentioned above, the openings in the backside of the cantilever are etched in two steps. In the first etching procedure, the hole is opened and in the second the cantilever thickness is reduced, leading to a simultaneous

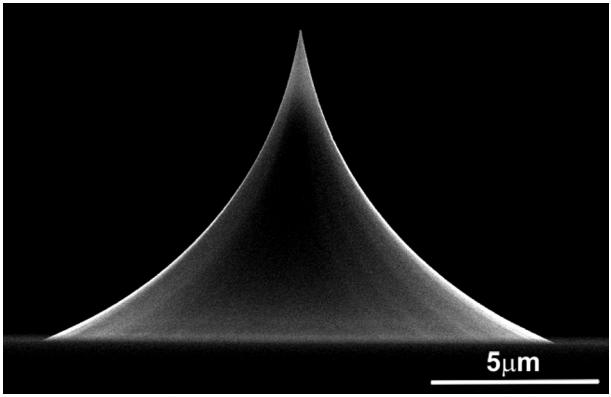

Figure 2.9: SEM image of a $Si0_2$ tip integrated on a silicon cantilever. The tip height is about 11μm.

enlarging of the hole. As depicted in Fig. 2.10 the final shape of the opening is about 5μm square near the tip base and approximately 18μm at its bigger end.

To test the probes for AFM imaging, images in contact mode were performed on a commercial microscope [1]. A latex bead projection pattern, so-called Fischer pattern, was employed as sample [11]. This kind of sample consists of a glass substrate on which is deposited a monolayer of hexagonal close packed latex spheres. The latex beads are used as a mask for physical vapor deposition. After the deposition of approximately 20nm of aluminum, the spheres are dissolved and small triangular metal islands remain on the glass substrate. On the contact mode image shown in Fig. 2.11, the metal triangles as well as some lattice defects are clearly seen. The measured topographical resolution is comparable to that obtained with commercial AFM probes.

[1] Nanoscope III from DI

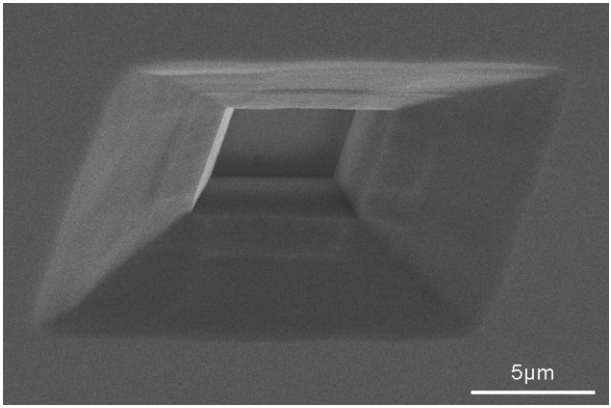

Figure 2.10: SEM image of the backside of a silicon cantilever. The hole positioned just underneath the tip has been etched in two steps.

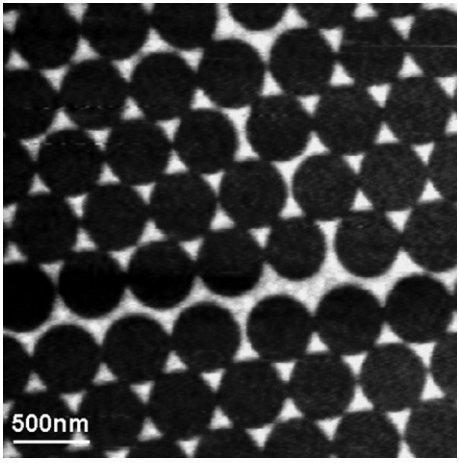

Figure 2.11: Contact mode AFM image of a latex bead projection pattern, so-called Fischer pattern. The hexagonal arrangement of the triangular metal islands are clearly seen.

2.5 NanoWorld probe design

For commercialization, the SNOM probe fabrication process is applied to the standard design of NanoWorld, the industrial partners of the project. Each probe consists of a body chip with only one cantilever on its end. The cantilever has a rectangular shape and is again 80μm wide and 3μm thick. The length of the lever is 525μm leading to a calculated spring constant of 0.6N/m and resonance frequency of 15kHz.

2.5.1 Improvement of the fabrication process

The most critical step in the fabrication procedure is the realization of the backside hole into the cantilever. As already mentioned in section 2.3.3 it is necessary to use spray resist coating in order to achieve photoresist deposition with high uniformity inside the deeply etched cavities. Moreover, to be able to get well defined patterns inside these cavities, the exposure of the photoresist has to be performed with a projection aligner. Another aspect is the alignment between the backside hole and the frontside tip. Due to internal stress, a 3μm thick membrane is deformed due to internal stress. When performing the photolithography on such a membrane, this deformation can cause a misalignment of the hole respective to the tip. The thinning down of the cantilever explained in section 2.3.4 makes it possible to perform this lithography on a thicker membrane, e.g. of 5μm thickness, which is less stressed. Thus, the misalignment between hole and tip is highly reduced.

A further process improvement would be the simultaneous patterning of the hole and of the cantilever in one single photolithography step. In this case, the lithography step for the cantilever definition (section 2.3.2) is skipped. Instead, the cantilever structuring is proceeded together with the backside hole fabrication. Again, a projection aligner is used to get a high definition of the patterns - cantilever and hole - inside the deep cavities. The cantilever is then released in the same KOH etching step as the hole is opened. This process improvement permits to avoid one lithography step and thus reduce the processing costs.

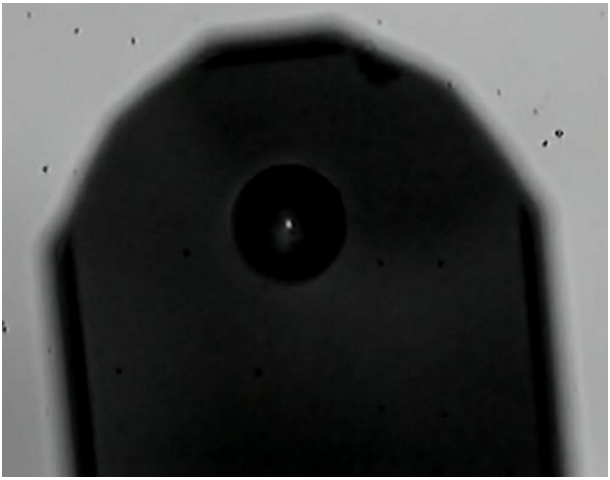

Figure 2.12: Image of the light transmitted through a fully aluminum coated $Si0_2$ tip. This top view of the cantilever shows the light emitted from the tip when illuminated with a laser beam from the back.

2.6 Light transmission through fully metal coated tips

As mentioned above, the tips are completely covered with a nominally 100nm thick metal layer. Although no aperture in the metal coating is post-processed at the tip apex, light is transmitted through the probe. Figure 2.12 shows the top view of the end of a cantilever with an integrated, fully metal coated $Si0_2$ tip. The cantilever is illuminated from the backside with a laser beam (λ=532nm). The transmitted light spot is clearly visible on this picture.

The mechanism of light transmission through the probes is not understood. A $\sim$60nm thick aluminum layer would be opaque when deposited on a flat surface. The goal of the next chapters is to study this phenomenon in more detail. Several far-field and near-field experiments were performed to get indications on the transmission mechanism of the light through the entirely metal coated probes.

2.7 Fluorescence tip calibration sample

During SNOM imaging, the topography is recorded simultaneously with the optical image. The motion of the tip normal to the sample surface caused by the tip to sample distance control mechanism often leads to undesirable crosstalk in the near-field optical images. In fact, in contact mode, the tip follows the topography of the sample. To this end, the tip has to move vertically for changing the tip to sample distance, and consequently the intensity of the optical signal varies. This crosstalk between topography and optical information generates features in the optical image that are correlated with the structures in the topographical image [12, 13, 14]. To avoid these topography induced artifacts and test the "true" optical resolution of SNOM probes, topography-free samples can be used [15].

We fabricated a simple characterization sample with no correlation between topography and optical signal based on local bleaching of a fluorescent layer with an electron beam. For this purpose, a glass cover slit covered with a thin layer of indium tin oxide (ITO) was spin coated with a 10^{-5}M diluted solution of succinimidyl esters of the Alexa Fluor 532 dyes [2]. The ITO layer allows the discharging of the glass cover plate during the e-beam writing. Different structures were exposed, such as lines with different widths. As shown later in chapter 4, simultaneous recording of the topography and near-field optical image shows no topographical contrast correlated with the optical features. Thus, we can be sure that the contrast seen in the optical near-field image is a pure optical signal.

2.8 Summary and conclusions

The fabrication procedure of cantilever based SNOM probes proposed by Schürmann *et al.* [2] has been reconsidered and improved in view of reproducibility and yield. 11μm high $Si0_2$ tips integrated on silicon cantilevers could successfully be batch processed. Behind the tip a hole etched in the cantilever permits the light to be focused into the tip. In particular, the very

[2] Molecular Probes, Inc., 29851 Willow Creek Road, Eugene, OR 97402

critical step of quartz wafer bonding and thinning presented by Schürmann *et al.* could be eliminated. The fabrication process has been optimized and stabilized in order to meet industrial standards.

The $Si0_2$ tip radius could be very well controlled and high uniformity across the wafer could be shown. Before metallization, the tips show tip radii of few nanometers, similar to standard silicon AFM tips.

The $Si0_2$ tips are entirely covered with a metal layer and no aperture is manufactured at the tip apex. In any case, the probes show high light transmittance. A huge advantage of such a probe, is the small radius of the tip apex, providing a much higher topographical spatial resolution than that of conventional aperture probes. To investigate the mechanism of light transmission through our fully metal coated tips, several experiments were performed. The next chapters deal with the far-field and near-field characterization of the probes.

A topography-free fluorescence sample was fabricated to test the optical resolution of the SNOM probes. The idea is to bleach locally a fluorescent layer by means of an electron-beam.

Bibliography

[1] G. Schürmann. *Microfabrication of combined Scanning Near-field Optical and Scanning Force Microscopy probes*. PhD thesis, University of Neuchâtel, Institute of Microtechnology, Switzerland, (2000).

[2] G. Schürmann, W. Noell, U. Staufer, N. F. de Rooij, R. Eckert, J. M. Freyland, H. Heinzelmann. *Fabrication and characterization of a silicon cantilever probe with an integrated quartz-glass (fused-silica) tip for scanning near-field optical microscopy*. Appl. Optics **40**, 5040 (2001).

[3] R. Eckert, J. M. Freyland, H. Gersen, H. Heinzelmann, G. Schürmann, W. Noell, U. Staufer, N. F. de Rooij. *Near-field fluorescence imaging with 32nm resolution based on microfabricated cantilevered probes*. Appl. Phys. Lett. **77**, 3695 (2000).

[4] M. Madou. *Fundamentals of microfabrication*. CRC Press LLC, (1997).

[5] T. R. Albrecht, S. Akamine, T. E. Carver, C. F. Quate. *Microfabrication of cantilever styli for the atomic force microscope*. J. Vac. Sci. Technol. A **8**, 3386 (1990).

[6] O. Wolter, T. Bayer, J. Greschner. *Micromachined silicon sensors for scanning force microscopy*. J. Vac. Sci. Technol. B **9**, 1353 (1991).

[7] V. G. Kutchoukov, J. R. Mollinger, A. Bossche. *New photoresist coating method for 3-D structured wafers*. Sens. Actuators **85**, 377 (2000).

[8] P. P. Nga, P. M. Sarro, J. N. Burghartz. *IC-compatible process for pattern transfer in deep wells for integration of RF components*. Proc. SPIE Int. Soc. Opt. Eng. **4174**, 390 (2000).

[9] N. P. Pham, T. L. Scholtes, R. Klerk, B. Wieder, P. M. Sarro, J. N. Burghartz. *Direct spray coating of photoresist for MEMS applications*. Proc. of SPIE **4557**, 312 (2001).

[10] A. Suriadi, T. Luxbacher. *Photolithography on micromachined 3D surfaces using spray coating technology of photoresist*. Proc. of SPIE Int. Soc. Opt. Eng. **4404**, 245 (2001).

[11] U. C. Fischer, H. P. Zingsheim. *Submicroscopic pattern replication with visible light*. J. Vac. Sci. Technol. **19**, 881 (1981).

[12] B. Hecht, H. Bielefeldt, Y. Inouye, D. W. Pohl, L. Novotny. *Facts and artifacts in near-field optical microscopy*. J. Appl. Phys. **81**, 2492 (1997).

[13] R. Carminati, A. Madrazo, M. Nieto-Vesperinas. *Optical content and resolution of near-field optical images: Influence of the operating mode*. J. Appl. Phys. **82**, 501 (1997).

[14] P. G. Gucciardi, M. Colocci. *Different contrast mechanisms induced by topography artifacts in near-field optical microscopy*. Appl. Phys. Lett. **79**, 1543 (2001).

[15] T. Kalkbrenner, M. Graf, C. Durkan, J. Mlynek, V. Sandoghar. *High-contrast topography-free sample for near-field optical microscopy*. Appl. Phys. Lett. **76**, 1206 (2000).

Chapter 3

SNOM probe far-field characterization

In the previous chapter, the fabrication process of cantilever based scanning near-field optical microscopy probes has been presented. At the end of the fabrication run, a metal layer is deposited on the $Si0_2$ tips. As has been verified on several tips using transmission electron microscopy, this metal film covers the full tip. The image displayed in Fig. 3.1 shows that the probe is typically covered with 60nm of metal, when using a process that results nominally to 100nm on a flat wafer.

The goal of this study is to investigate the mechanism that allows the electromagnetic field to penetrate such a thick metal layer, which is opaque when deposited on a flat surface. The shape and size of the tips, the light coupling, the illumination characteristics or the type and thickness of the metal coating are parameters that influence the light emission from the tip. A certain amount of information about the optical behavior of these probes can be obtained, by analyzing, in the far-field, the light transmitted through the probes.

Before presenting the different far-field characterization experiments, some important results of theoretical calculations are presented in the first section of this chapter. These theoretical investigations were conducted by

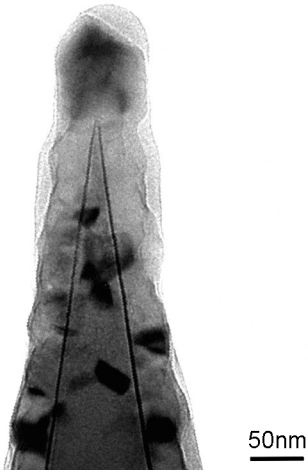

Figure 3.1: Transmission electron microscopy image of a completely aluminum coated $Si0_2$ tip. Nominally 100nm of metal was deposited in "planetary" mode. Prior to aluminum evaporation a 5nm thick layer of titanium was deposited as an adhesion layer.

L. Vaccaro [1]. I provided experimental measurements and realistic parameters for establishing the theoretical model.

3.1 Theoretical calculations

In a theoretical study, the propagation and the emission properties of the probes are investigated. The simulations are performed considering an iridium coated tip and are described in detail by Vaccaro *et al.* [1]. It has to be noticed, that the same qualitative results are obtained for an aluminum tip coating. However, for both metals, there is a large discrepancy of several orders of magnitudes between the calculated and measured values of the optical transmittance through the tip. An explanation for this divergence can be found in the Drude model [2] used for simulating the metal coating. Indeed, the real aluminum coating observed in the TEM picture of Fig. 3.1 is far from being an electron gas. Because the quantitative discordance between experiments and theory is less important for an iridium coating, this metal is preferred to present this theoretical model.

The calculations are based on the finite integration code MAFIA4 [2]. The investigated structure consists of a $Si0_2$ cone-like tip entirely coated with a 60nm thick layer of iridium. In such a structure, two propagating eigenmodes of the electromagnetic field can be distinguished. These two modes are separately coupled into the tip structure. The first mode is classified as a linearly polarized mode LP_{01}. The electric field directions and intensities calculated at increasing distances above the tip apex are displayed in Fig. 3.2. In this case, the electric field propagation remains perpendicular to the direction of propagation throughout the whole tip. When cutoff conditions are reached, the light leaks at the tip flank. In this situation the field confinement at the tip apex is very poor, as shown in Fig. 3.2d), where two large intensity lobes originating from the probe sides can be observed. At 400nm from the tip apex (Fig. 3.2c)) the polarization direction is the same as that of the injected light (Fig. 3.2a)).

[1] Applied Optics Laboratory, Institute of Microtechnology, University of Neuchâtel
[2] CST, Darmstadt, Germany

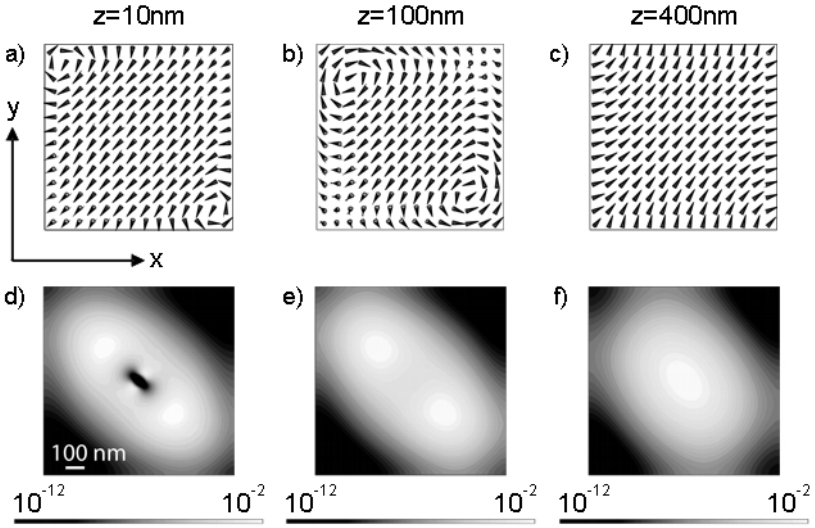

Figure 3.2: Theoretical calculations of the electric field direction (images a),b) and c)) and intensity contour plot (images d), e) and f)) for the LP_{01} mode at different heights above the tip apex. The pictures represent a square area of 900 x 900 nm^2.

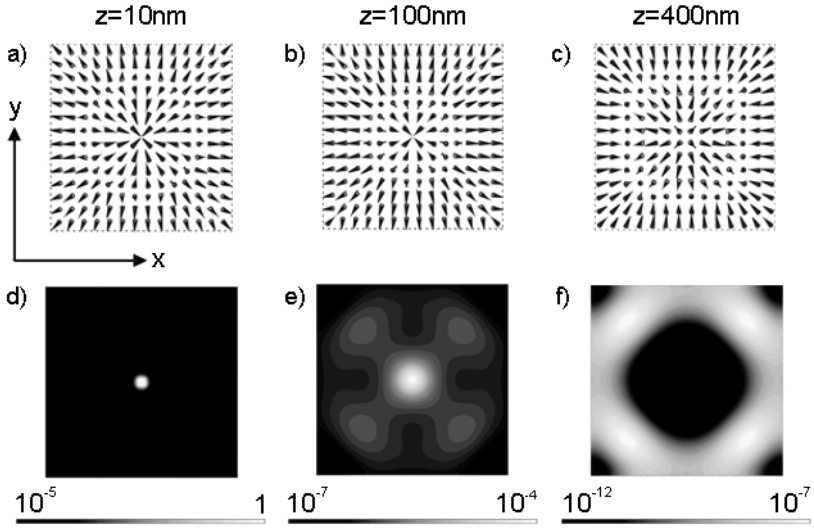

Figure 3.3: Theoretical calculations of the electric field direction (images a),b) and c)) and intensity contour plot (images d), e) and f)) for the LP_{11} mode at different heights above the tip apex. The pictures represent a square area of 900 x 900 nm^2.

The second mode, obtained by the superposition of two orthogonal LP_{11} modes, is characterized by a radial polarization. In this case, there is a non-vanishing z component of the electric field in the probe structure and this component is preserved in the near- and mean-field. These propagating conditions permit the coupling of bulk modes in the metal coating, and induce there stable waveguide conditions. Novotny and Hafner [3] came to similar conclusions in their theoretical analysis of cylindrical optical waveguides with finite real metal cladding. A high field confinement is induced at the tip apex, resulting in a subwavelength sized intensity peak in the near-field (Fig. 3.3d)). This small spot evolves into a larger one surrounded by four lobes that become dominant in the far-field (Fig. 3.3f)).

Further, a parametric study as a function of the diameter of the probe apex demonstrates that the field confinement, obtained when the electric field gets a strong component along the probe axis, strongly depends on the volume of the very apex of the tip.

Moreover, it can be deduced that the highest transmission corresponds to the sharpest structure, i.e. displaying a small cone angle. This finding is in contradiction with some earlier calculations [4, 5], where an enhanced transmission is theoretically predicted for higher cone angles. In that case, tips with a mechanical aperture are considered. This suggests that in the case of fully metal coated tips, the transmission of light is largely based on mechanisms other than those governing conventional aperture SNOM probes.

3.2 Polarization investigations in the far-field

In order to investigate the tips optically, their far-field emission patterns has been observed. For that purpose, a simple optical set-up has been realized as described in the next paragraph.

3.2.1 Experimental set-up

By means of an objective lens (20x, NA 0.35), a linearly polarized helium-neon laser beam (λ=633nm) is focused, from the backside, into the tip (Fig.

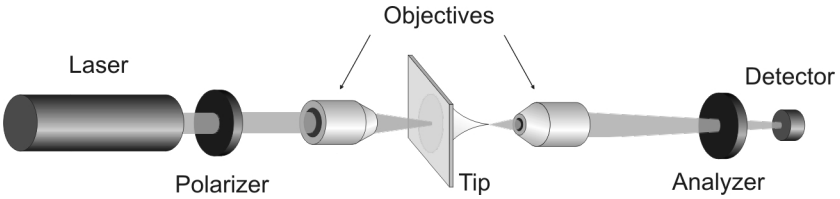

Figure 3.4: Set-up used for the far-field optical characterization of the probes. A laser beam is focused into the tip from the backside with an objective lens. The light emitted from the tip is collected by a second objective and projected on a detector.

3.1). The emitted signal is collected using a second microscope objective (100x, NA 0.9). The light that passes through the probe is then analyzed with a CCD camera or a photodiode. Polarizing filters can be placed between the laser source and the first objective as well as between the second objective and the detecting system. The intensity of the illumination can be regulated with the first filter. By varying the direction of the second polarizer, the polarization properties of the tips can be investigated. This experimental set-up is schematically depicted in Fig. 3.4.

3.2.2 Far-field emission patterns

Far-field characterization of the probes emission has been performed by coupling a linearly polarized laser beam (λ=633 nm) into the tips. The pattern displayed in Fig. 3.5a) has been recorded in a configuration in which the polarizer and the analyzer are parallel. The emitted radiation displays a polarization state parallel to the one of the field that has been coupled into the probe. A homogeneous diffraction far-field pattern is obtained that resembles an Airy disk. Figure 3.5b) shows the intensity pattern recorded when the polarizer is orthogonally oriented relatively to the analyzer. In this case, no total extinction occurs, and the emission pattern shows a four-fold "clover" symmetry. Calculations of the emission pattern of a round metallic aperture, as seen with the above described optical set-up [6], are in good agreement with the patterns of Fig. 3.5. Further, for fiber based aperture probes with a circular aperture, the same four-fold pattern can be observed

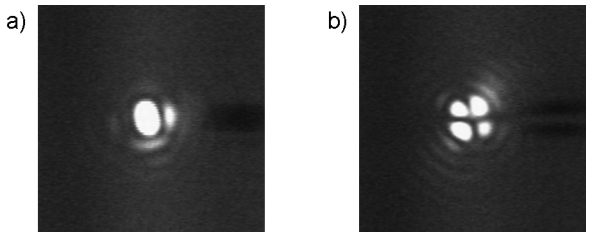

Figure 3.5: Far-field emission patterns of a fully metal coated $Si0_2$ tip: Intensity of polarized light, transmitted through the tip with parallel (a) and crossed (b) polarizer and analyzer.

for crossed polarizers [7].

By comparing these polarization dependent far-field emission patterns with the theoretical calculations discussed above, it is expected that the injection of linearly polarized light into the tip would lead to linearly polarized light emission observed in the far-field. This is obviously not the case, since no extinction occurs for the experimental configuration with crossed polarizers. This suggests that even if one single mode radiation is coupled into the tip, another mode is generated at its entrance or exit. We assume that the two experimentally observed polarization states can be understood in terms of the LP_{01} and LP_{11} modes propagating through the tip. If so, both modes are excited when a linearly polarized laser light is injected into the probe.

3.3 Transmittance measurements

For standard fiber based SNOM probes calculated as well as measured typical transmission values of apertures around 100nm in diameter were found to be in order of 10^{-6} to 10^{-5} [8, 9]. Although the probes are produced under identical conditions, they exhibit significant differences in transmission efficiency, what is largely due to variations of the taper shape [8]. Cantilever based SNOM probes, consisting of a hollow pyramidal shaped metal tip integrated in a conventional silicon cantilever, show a much higher transmission

ratio, in the order of 10^{-3} for aperture sizes around 110nm [10].

Our SNOM probes show high optical transmission even if they are fully covered with a rather thick metal film. For transmittance measurements the optical set-up described in section 3.2.1 was used. The transmittance was characterized by the ratio of the light power passing through the set-up, with and without the tip in the optical path. For practical reasons, the experiments were carried out on tips in arrays made of fused silica wafers rather than on cantilever-mounted tips. These arrays of 500x500 tips, separated by 17μm are fabricated according to the process described in paragraph 2.2.

By optimizing the optical properties of the probe, for example by choosing the optimal tip shape or metal coating, maximum light transmission and minimum spot size should be achieved, in view of high topographical and optical resolution and high optical signals. Therefore, the influence of the metal coating and of the tip cone opening angle on transmittance was investigated.

3.3.1 Different metal coatings

In a first set of experiments, nominally 100nm of various metals was evaporated onto the different tips in the so-called "planetary" mode (see also section 2.3.5). A thin adhesion layer of 5nm thick titanium was deposited on the tips prior to the metal evaporation (except for chromium). The resulting film thickness at the tip apex is in the range of 60nm similar to the one shown in Fig. 3.1. As metal, we chose aluminum for its excellent optical properties, iridium and chromium for their hardness, potentially increasing the lifetime of the probes, and gold for its plasmon-related properties [11]. Each bar on the graph in Fig. 3.7 represents the mean value of the transmittance as measured with a variety of 50 different tips. The observed transmittance differences correlate with the skin depth [3] values (Fig. 3.6) for these metals, meaning that chromium showed the highest transmittance, followed by gold, iridium and aluminum (Fig. 3.7). Note, that the situation for gold is ambiguous since this metal shows resonances at these wavelengths.

[3] The skin depth is the distance at which an electromagnetic wave can penetrate the metal until its intensity is reduced to a value of $1/e^2$ of the input intensity.

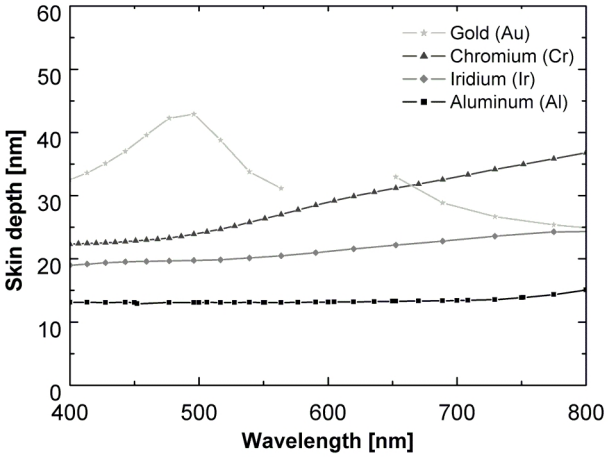

Figure 3.6: Skin depth values of aluminum, iridium, gold and chromium versus the illumination wavelength. Values found in the literature (database by Sopra SA).

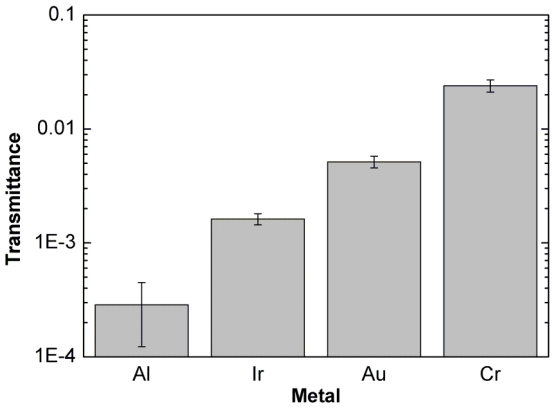

Figure 3.7: Light transmittance measurements on tips in arrays, through tips coated with, respectively, aluminum, iridium, gold and chromium. The tips have an opening angle of 55˚ and the laser wavelength is 633nm. Each bar in the graph represents the mean value of transmittance measurements of 50 different tips.

3.3.2 Different cone opening angles

In a second set of experiments, tips with cone opening angles of 97°, 55° and 30° were compared in view of light transmittance. For this purpose, nominally 100nm of iridium was evaporated on the tips, in "planetary" mode. Figure 3.8 shows that a smaller tip angle leads to a higher transmittance. This trend could be demonstrated for all tested coating metals. Furthermore, the finite element model simulations described in paragraph 3.1 reproduce the tendency of the measurements.

The measured transmittances are surprisingly high compared with the values found in the literature for conventional aperture probes. For an aluminum coating, for example, transmittances of 10^{-3} to 10^{-4} are obtained, whereas values of 10^{-6} to 10^{-5} are reported in the literature for fiber based probes. This high optical throughput can not be explained in terms of residual light transmission through the finite metal layer, which is calculated to be in the order of 10^{-5} for a 60nm thick aluminum film.

This suggests that the tip apex could give rise to a field enhancement, providing conditions similar to those in the so-called apertureless SNOM configuration (see also paragraph 1.2.2).

It is well known that strong field confinement can be achieved in the vicinity of small particles and sharp tips [12]. These phenomena could be successfully applied for near-field optical imaging [13, 14, 15] or surface-enhanced Raman scattering [16]. In particular, it has been demonstrated that very strong field gradients can be produced at the tip apex, when the excitation wavelength is such that plasmon resonances are excited [17, 18]. But, it is also possible to create intense optical field gradients at the tip apex without having recourse to plasmon resonances (lightning rod effect) [19, 20]. The lightning rod effect provides a much weaker intensity enhancement, reaching, for example for a silver particle, 70 at an illumination wavelength of 600nm [20]. Calculations [19] and experimental work [21, 22, 23] have shown that in this case, the total field intensity is dominated by the role played by the vertical field component of the scattering at the tip.

Considering the two effects described above and in paragraph 3.1, i.e.

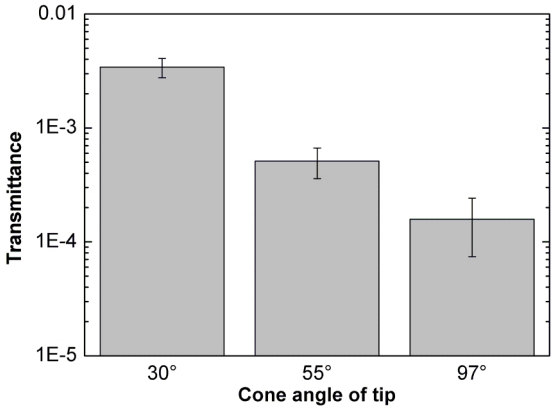

Figure 3.8: Light transmittance measurements on tips in arrays, through tips coated with nominally 100nm of iridium for tip opening angles of 30˚, 55˚ and 97˚. The laser wavelength is 633nm. Each bar in the graph represents the mean value of transmittance measurements of 50 different tips.

the coupling to modes in the metal coating and the optical field enhancement at the tip apex, high optical throughput of a fully metal coated tip can be explained. Similarly, Yatsui *et al.* [24] reported high optical throughput of a completely aluminum coated pyramidal silicon tip. However, direct comparison with our results is difficult because of the different tip parameters, materials or illumination conditions implemented in their experiments.

3.3.3 Different metallizations

Typical deposition of the metal coating on the SNOM probes is performed by evaporation in the so-called "planetary" mode (see 2.3.5). All of the above presented measurements have been performed on tips that have been metallized with this evaporation procedure. Additionally, an adhesion layer of 5nm thick titanium was deposited prior to the metal deposition (except for chromium).

In order to study the role of the adhesion layer on the light transmission mechanism through the SNOM probes, the transmittances through aluminum coated probes, with and without adhesion layer have been investigated. A difference in transmittance of one order of magnitude could be demonstrated. In fact, the tips covered with aluminum without previous deposition of the adhesion layer show a 10 times smaller transmittance. For analyzing this phenomena more in detail, three different metallization procedures have been investigated by imaging the coated tips in a transmission electron microscope.

By evaporating a 5nm thick titanium adhesion layer followed by 100nm of aluminum in "planetary" mode, the resulting metal film is composed of well ordered metal grains arranged along the tip flanks as shown on the transmission electron microscope image of Fig. 3.9a). Additionally, it can be observed that the titanium adhesion layer is amorphous, whereas the aluminum grains are crystalline. When depositing 100nm of aluminum, again in "planetary" mode, without the titanium adhesion layer the resulting metal grain arrangement looks more random. In this case, the interface between the tip core and the coating can hardly be seen on the TEM picture displayed in Fig. 3.9b). In a third tested metallization procedure, 100nm of aluminum was evaporated in the "normal" mode, i.e. the wafers stay normal to the evaporation direction, without adhesion layer. The grain arrangement become more random again (Fig. 3.9c)). In this case, the metal grains are not oriented along the tip walls anymore, increasing the roughness of the lateral surfaces of the tip. The surface roughness of the tip flanks has been estimated from the TEM images. For each metallization process, three probes have been considered in order to estimate the roughness average of the coating (table 3.1). It has to be noticed that despite the different metallization processes, the very apex of the tip consists of a final metal grain, that has similar size and shape.

From the above observations, it is obvious, that the variation of the light throughput of the probes, is not due to the presence of the adhesion layer, but rather to its consequences on the resulting metal grain distribution.

Metallization	5nm Ti/100nm Al "planetary" mode	100nmAl "planetary" mode	100nm Al "normal" mode
R_a of tip flanks	1.9nm±0.7nm	2.5nm±0.7nm	5.9nm±1.5nm

Table 3.1: Roughness average of the aluminum coating at the tip walls for different metallization processes. For each process, the roughness values were estimated from transmission electron microscope images of three different tips.

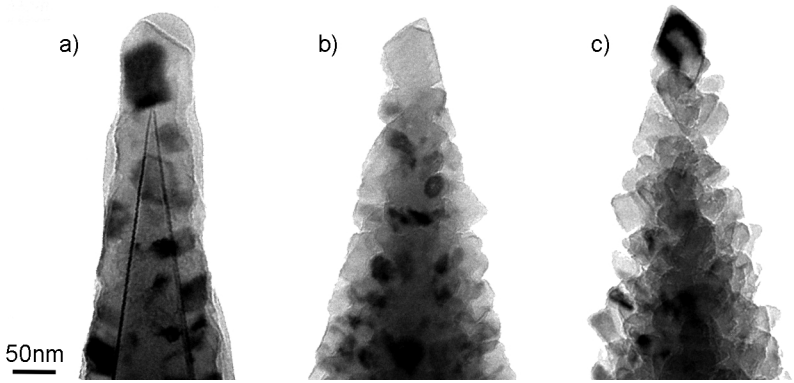

Figure 3.9: Transmission electron microscope images of Al-coated SNOM tips fabricated under different metallization conditions. a) The tip was metallized with 5nm of Ti and 100nm of Al in the "planetary" mode. b) The tip was metallized with 100nm of Al in the "planetary" mode. c) The tip was metallized with 100nm of Al in the "normal" mode.

3.4 Spectroscopic characterization

As mentioned in the previous paragraphs, especially high field gradients can be achieved at the apex of a sharp metal tip, when plasmon resonances are excited. For determining if, in the present study, the high light throughput of the probes is due to plasmon excitation, a study of the spectral properties of light transmitted by the SNOM probes has been analyzed [4].

For that purpose, the same tip arrays as those used for the transmittance measurements were illuminated with white light [5] and imaged using a high NA confocal microscope. Part of the detected light was analyzed by means of a spectrometer. Spectra of the light passing through the tips as well as of the light passing through the flat metal layer between the tips have been measured. Different metals and coating thicknesses have been probed. The lamp spectrum was subtracted and the curves normalized.

The different spectra are shown on Fig. 3.10. The curves of the spectra taken on the tips and on the flat coating are very similar one to each other. The small differences found between spectra may be caused by inhomogeneities or defects in the metal coating. In particular, for gold, the difference between the curves are due to slight changes of the coating thickness.

No resonance effects could be observed in the spectra, neither for gold nor for silver, which have sharp plasma resonances in the visible spectrum [25]. Indeed, theoretical calculations [6] show that for gold and silver deposited on $Si0_2$, plasmon resonances can occur in the Kretschmann configuration [27] at the experimentally used wavelengths (532nm and 633nm). For aluminum, however, no excitation of surface plasmon is expected at these wavelengths.

[4] The spectroscopic measurements have been performed in collaboration with Prof. A. J. Meixner and Dr. H. Kneppe from the University of Siegen.

[5] Thungsten lamp

[6] Rigorous coupled wave analysis RCWA [26] performed by E. Descrovi, Applied Optics Laboratory, Institute of Microtechnology, University of Neuchâtel

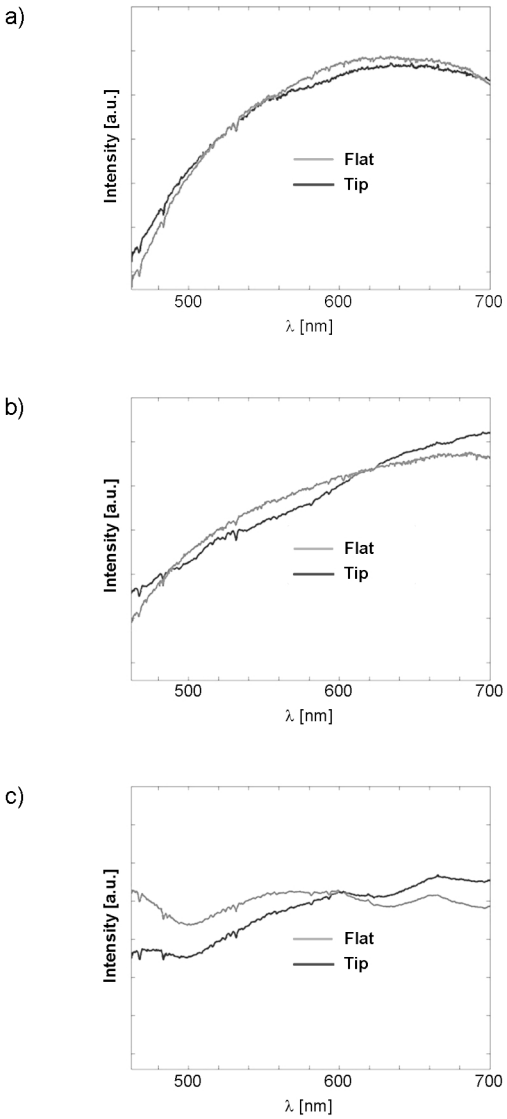

Figure 3.10: Spectroscopy measurements of different metal coatings. The white light illumination is performed with a thungsten lamp. For each metal, a spectra of the coated tip, and of a flat surface coated with the same metal, is shown: a) 75nm thick aluminum layer, b)100nm thick silver layer, c) 100nm thick gold layer.

3.5 Temperature characterization

The thermal behavior of fiber based SNOM probes has been studied some years ago [28, 29]. During SNOM experiments, most of the light input to the probe is either back reflected or absorbed, which can result in a dramatic temperature increase. For fiber probes, 1mW laser power is already increasing the probe temperature significantly. It has been shown that even though the aluminum melting temperature is around 650°C, the tip coating cannot bear more than 450° without damage [29]. The difference of the thermal expansion coefficients of the aluminum and the silica plays a central role in the temperature limit. Moreover, it has been shown [30], that the absorption of light in the fiber tip significantly influences the image formation in shear-force mode (see also section 1.2.3).

From these earlier experiments, we could also expect high tip temperatures during illumination of our SNOM probes. This temperature increase could affect the light transmission through the probes, by changing the grain structure of the metal coating and thus opening small channels or pinholes for the light. Moreover, one can imagine that enhanced oxidation or even evaporation of the metal could occur.

3.5.1 Miniaturized thermocouple

In order to measure the temperature of the SNOM probes, a thermoelectric sensor whose active region is small enough to fit the dimension of the tip was used (Fig. 3.11).

This miniaturized thermocouple is made of welded wires of platinum and platinum-rhodium 10% (S-type). This technique has already been used to study the thermal behavior of metal-coated fiber tips [31] [7].

For this purpose, a SNOM probe was mounted in an optical set-up similar to that described in paragraph 3.2.1. When the laser was well focused into the tip, the small thermocouple, which was mounted on a x-y-z micropositioning table, was approached. The whole procedure was done under

[7] The temperature measurements were done in collaboration with L. Thiery from CREST in Belfort.

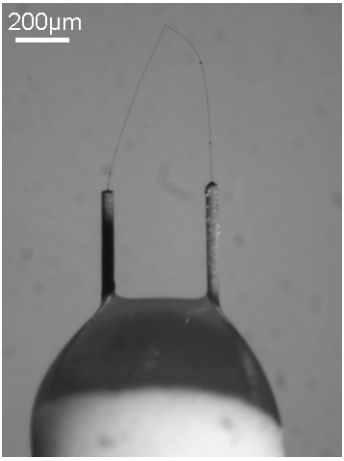

Figure 3.11: Miniaturized thermocouple used to measure the temperature of the tip during illumination.

a microscope to position the thermocouple in contact with the tip. After setting the position of both sensor and tip, the temperature measurement was performed for variable illumination laser power.

3.5.2 Temperature measurement results

The graph of Fig. 3.12 shows the temperature measurements as function of the laser input power (λ=532nm). A maximum temperature of approximately 160˚C for 10mW input laser power is reached. This value is far below the measured temperature for fiber based probes. We assume that unlike silica fibers, the large thermal conductance of our silicon cantilever prevents large heating of the tip. At these moderate temperatures, it is unlikely that the tip coating would be deteriorated by thermal effects.

Nevertheless, it has to be noticed that for such measurement it is difficult to have a good thermal contact and a minimal perturbation of the temperature distribution at the same time. Although the contact point of the sensor was on the tip flank and not at the very apex of the tip, it is possible to have measurement errors due to cooling effects induced by the junction contact,

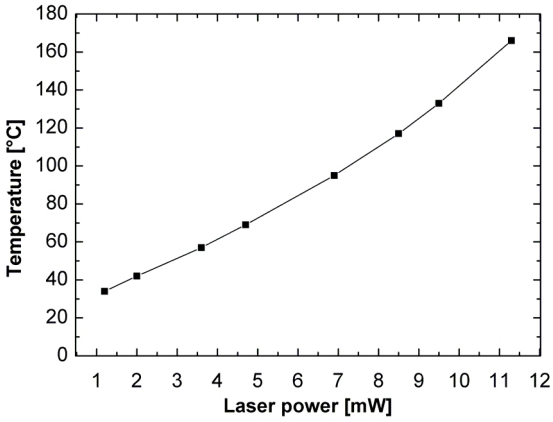

Figure 3.12: Temperature measurements as a function of the laser input power performed using a miniaturized thermocouple. The laser wavelength is 532nm.

or due to direct illumination of the junction.

To be sure of our conclusion that the metal coating is not affected, the aluminum-coated tip apex was examined with a transmission electron microscope before and after illumination.

3.5.3 TEM characterization

Figure 3.13a) shows the transmission electron microscope image of a probe similar to that shown in Fig. 3.1. The TEM image of the same tip that has been illuminated during 30 minutes with 10mW laser light is displayed in Fig. 3.13b). Clearly, the metal coating remained intact during illumination and no change in the polycrystalline structure of the aluminum occurred. This result confirms the above discussed temperature measurements.

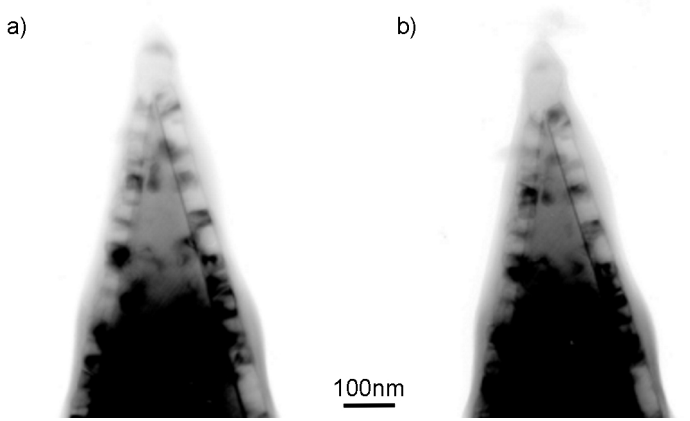

Figure 3.13: a) Transmission electron microscope image of an Al-coated $Si0_2$ tip prior to SNOM measurements. b) Transmission electron microscope image of the tip after illumination of the tip with 10mW input laser power. The laser wavelength is 633nm.

3.6 Summary and conclusions

By carrying out different far-field characterization experiments, one can draw some conclusions about the optical behavior of the fully metal coated $Si0_2$ tips.

Finite element simulations show that there are two propagating modes in the tip structure, which show a very distinct behavior when coupled separately into the probe. Subwavelength confinement of the electromagnetic field occurs when the electric field gets a strong component along the axis of the probe. This situation is achieved when radially polarized radiation is coupled into the tip. Experimentally, by coupling a linearly polarized laser beam into the tip, very pronounced far-field emission characteristics can be observed, when polarizers, positioned in front of the cantilever entrance and behind the tip apex, are either parallel or crossed by 90 degrees. It can be concluded that, even if only a single mode radiation is coupled into the probe, other excited modes can be generated at its entrance or exit.

Moreover, the computational results, backed up with experimental work,

demonstrate that a sharper tip leads to higher transmitted light power. This is the inverse behavior of aperture SNOM probes, for which the light transmission decreases with decreasing cone opening angle.

Furthermore, a high light transmittance through the tip apex could be demonstrated experimentally for different coating materials. In order to investigate the origin of this high transmittance, the spectroscopic behavior of the tips has been analyzed. This spectral study excludes field enhancement at the tip apex due to plasmon resonances. Tip enhancement effects due to lightning rod effects, similar to those observed in the apertureless SNOM configuration, are assumed. In fact, in both cases, the emitted light is strongly dependent on the vertical field component at the tip apex.

A huge advantage of using fully metal coated tips compared with standard aperture probes, is the small apex radius of about 30nm, which provides high topographical resolution. Another benefit of our SNOM probes is given by the low temperature of the tip during illumination. Working with really small apertures (<50nm) is often impossible since the transmittance decreases dramatically, which cannot be overcome by an increased input power that would lead to damage of the metal coating. This is the reason why most SNOM studies today are carried out with apertures of 80-100nm. In the case of fully metal coated probes, this problem could be circumvented. The measured temperature of the tip remains low, even for high light input power.

Bibliography

[1] L. Vaccaro, L. Aeschimann, U. Staufer, H.P. Herzig, R. Dändliker. *Propagation of the electromagnetic field in fully coated near-field optical probes*. Appl. Phys. Lett. **83**, 584 (2003).

[2] N. W. Ashcroft, N. D. Mermin. *Solid state physics*. Saunders college publishing, (1976).

[3] L. Novotny, C. Hafner. *Light propagation in a cylindrical waveguide with a complex, metallic, dielectric function*. Phys. Rev. E **50**, 4094 (1994).

[4] L. Novotny, D. W. Pohl, B. Hecht. *Scanning near-field optical probe with ultrasmall spot size*. Opt. Lett. **20**, 970 (1995).

[5] B. Knoll, F. Keilmann. *Electromagnetic fields in the cutoff regime of tapered metallic waveguides*. Opt. Comm. **162**, 177 (1999).

[6] G. Schürmann. *Microfabrication of combined Scanning Near-field Optical and Scanning Force Microscopy probes*. PhD thesis, University of Neuchâtel, Institute of Microtechnology, Switzerland, (2000).

[7] T. Lacoste. *Optische rasternahfeld-Mikroskopie mit Polarisationskontrast*. PhD thesis, University of Basel, Philosophisch-Naturwissenschaftlichen Fakultät, Switzerland, (1997).

[8] G. A. Valaskovic, M. Holton, G. H. Morrison. *Parameter control, characterization, and optimization in the fabrication of optical fiber near-field probes*. Appl. Opt. **34**, 1215 (1995).

[9] B. Hecht, B. Sick, U. P. Wild, V. Deckert, R. Zenobi, O. J. F. Martin, D. W. Pohl. *Scanning near-field optical micrsocopy with aperture probes: Fundamentals and applications*. J. Chem. Phys. **112**, 7761 (2000).

[10] S. Werner, O. Rudow, C. Mihalcea, E. Oesterschulze. *Cantilever probes with aperture tips for polarization-sensitive scanning near-field optical microscopy*. Appl. Phys. A **66**, 367 (1998).

[11] O. Sqalli, M.-P. Bernal, P. Hoffmann, F. Marquis-Weible. *Improved tip performance for scanning near-field optical microscopy by the attachment of single gold nanoparticle*. Appl. Phys. Lett. **76**, 2134 (2000).

[12] J. Wessel. *Surface-enhanced optical microscopy*. J. Opt. Soc. Am. B **2**, 1538 (1985).

[13] F. Zenhausern, M. P. O'Boyle, H. K. Wickramasinghe. *Apertureless near-field optical microscope*. Appl. Phys. Lett. **65**(13), 1623 (1994).

[14] P. Gleyzes, A. C. Boccara, R. Bachelot. *Near field optical microscopy using a metallic vibrating tip*. Ultramicroscopy **57**, 318 (1995).

[15] Y. Inouye, S. Kawata. *Reflection-mode near-field optical microscope with a metallic probe tip for observing fine structures in semiconductor materials*. Opt. Comm. **134**, 31 (1997).

[16] R. M. Stöckle, Y. D. Suh, V. Deckert, R. Zenobi. *Nanoscale chemical analysis by tip-enhanced Raman spectroscopy*. Chem. Phys. Lett. **318**, 131 (2000).

[17] W. Denk, D. W. Pohl. *Near-field optics: Microscopy with nanometer-size fields*. J. Vac. Sci. Technol. B **9**, 510 (1991).

[18] A. Kramer, W. Trabesinger, B. Hecht, U. P. Wild. *Optical near-field enhancement at a metal tip probed by a single fluorophore*. Appl. Phys. Lett. **80**, 1652 (2002).

[19] O. J. F. Martin, C. Girard. *Controlling and tuning strong optical field gradients at a local probe microscope tip apex*. Appl. Phys. Lett. **70**, 705 (1997).

[20] J. P. Kottmann, O. J. F. Martin, D. R. Smith, S. Schultz. *Non-regularly shaped plasmon resonant nanoparticle as localized light source for near-field microscopy*. J. Microscopy **202**, 60 (2001).

[21] L. Novotny, E. J. Sánchez, X. S. Xie. *Near-field optical imaging using metal tips illuminated by higher-order Hermite-Gaussian beams*. Ultramicroscopy **71**, 21 (1998).

[22] L. Aigouy, A. Lahrech, S. Grésillon, H. Cory, A. C. Boccara, J. C. Rivoal. *Polarization effects in apertureless scanning near-field optical microscopy: an experimental study*. Opt. Lett. **24**, 187 (1999).

[23] A. Bouhelier, M. Beversluis, A. Hartschuh, L. Novotny. *Near-field second-harmonic generation induced by local field enhancement*. Phys. Rev. Lett. **90**, 013903–1 (2003).

[24] T. Yatsui, K. Itsumi, M. Kourogi, M. Ohtsu. *Metallized pyramidal silicon probe with extremely high throughput and resolution capability for optical near-field technology*. Appl. Phys. Lett. **80**, 2257 (2002).

[25] R. G. Milner, D. Richards. *The role of tip plasmons in near-field Raman microscopy*. J. Microscopy **202**, 66 (2001).

[26] M. G. Moharam, T. K. Gaylord. *Rigorous coupled-wave analysis of planar-grating diffraction*. J. Opt. Soc. Am. **71**, 811 (1981).

[27] S. Kawata. *Near-field optics and surface plasmon polaritons*. Springer-Verlag, (2001).

[28] A. H. La Rosa, B. I. Yakobson, H. D. Hallen. *Origins and effects of thermal processes on near-field optical probes*. Appl. Phys. Lett. **67**, 2597 (1995).

[29] M. Stähelin, M. A. Bopp, G. Tarrach, A. J. Meixner, I. Zschokke-Gränacher. *Temperature profile of fiber tips used in scanning near-field optical microscopy*. Appl. Phys. Lett. **68**, 2603 (1999).

[30] C. Lienau, A. Richter, T. Elsaesser. *Light-induced expansion of fiber tips in near-field scanning optical microscopy*. Appl. Phys. Lett. **69**, 325 (1996).

[31] L. Thiery, N. Marini, J.-P. Prenel, M. Spajer, C. Bainier, D. Courjon. *Temperature profile measurements of near-field optical microscopy fiber tips by means of sub-micronic thermocouple*. Int. J. Therm. Sci. **39**, 519 (2000).

Chapter 4

SNOM probe near-field characterization

High light transmission through completely metal coated $Si0_2$ tips has been demonstrated in the previous chapter. The far-field emission patterns of Fig. 3.5 suggest that the light emission of the tips is similar to that of commonly used fiber based aperture probes. However, a large optical throughput speaks in favor of an extended light source. Thus, additional experimental work has been carried out in order to study the optical resolution capabilities of the probes.

Moreover, as indicated by the theoretical work presented in the previous chapter, high field confinement should be induced at the tip apex under specific illumination conditions. Indeed, these simulations show that two modes can propagate in the tip, one giving rise to high field confinement in the near-field (LP_{11}), while the other one (LP_{01}) does not. Based on this model, ideal experimental conditions for high resolution imaging would be given by the excitation of the LP_{11} mode and the suppression of the LP_{01} mode.

This chapter focuses on the near-field characterization of the SNOM probes. For that purpose, results from different imaged samples are presented, as well as several experiments performed in relation with the illumination and light coupling conditions of the probes. Particular attention is paid to polarization aspects.

4.1 SNOM imaging

Different imaging experiments have been performed to determine the optical resolution of the SNOM probes. All the imaging experiments (except those taken in collection mode) shown in this work have been performed with an AlphaSNOM microscope from Witec GmbH [1]. The employed light source is a frequency doubled Nd:YAG laser with an emission wavelength of 532nm. For acquiring all the images presented in this section, fully aluminum coated tips have been used ("planetary" mode deposition of a nominally 5nm thick titanium adhesion layer followed by 100nm of aluminum).

A very convenient test sample is the so-called Fischer pattern [1]. However, as already mentioned in section 2.7, the small topographical variations of that kind of sample can, and usually do, give rise to undesired crosstalk in the near-field optical image. In order to avoid these topographical artifacts a special test sample has been manufactured (see section 2.7 for more details). The ultimate test for sensitivity and resolution of SNOM is the imaging of point-like light sources such as individual fluorescent labelled molecules. For that reason, the SNOM probes have also been tested on a single molecule sample.

4.1.1 Fischer pattern

The Fischer pattern test sample is a latex bead projection pattern. A densely packed monolayer of latex beads is deposited on a glass substrate and coated with a metal (for instance with a 20nm thick aluminum film). By removing the beads, a hexagonal array of metallic triangular islands remains on the substrate. If the bead diameter is 220nm, the final pattern will show metal islands of approximately 30nm in size, so that two neighboring islands are separated by 110nm.

Such a Fischer sample has been imaged in contact mode. The simultaneously recorded topography and near-field optical images are depicted in Fig. 4.1. The small metal islands are visible in the topography (Fig. 4.1a))

[1] WITec Wissenschaftliche Instrumente und Technologie GmbH, Hörvelsinger Weg 6, D-89081 Ulm, Germany

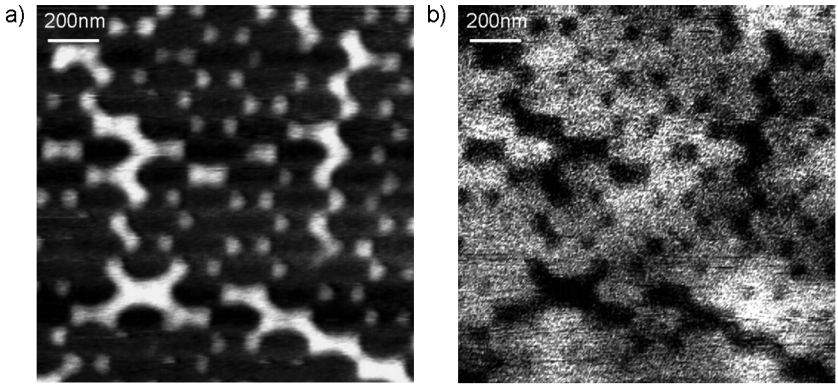

Figure 4.1: Simultaneously recorded topography (a) and near-field optical image (b) of a Fischer pattern acquired in contact mode. The mean distance between two adjacent metal islands is 110nm.

as bright spots and as dark spots on the optical image (Fig. 4.1b)). Some lattice defects can also be observed on both pictures. As neighboring metal islands are 110nm apart, the optical resolution is considerably better than 100nm.

However, this value given for the optical resolution might be influenced by topography artifacts. Different experiments have demonstrated strong correlations between the topography and the optical images in SNOM operation [2, 3]. In order to avoid topographical artifacts, the topography and the optical image have to be highly uncorrelated [2]. Therefore, more imaging experiments on fluorescence samples have been performed.

4.1.2 Fluorescence measurements

For estimating the "true" optical resolution obtainable with the probes, a specially developed sample has been manufactured. The fabrication of the sample is explained in section 2.7. The idea is based on the local bleaching of a fluorescent layer by means of an electron beam writer. Different structures have been exposed, in particular various lines of different widths. A sample comprising 100nm wide lines separated by 1μm has been imaged

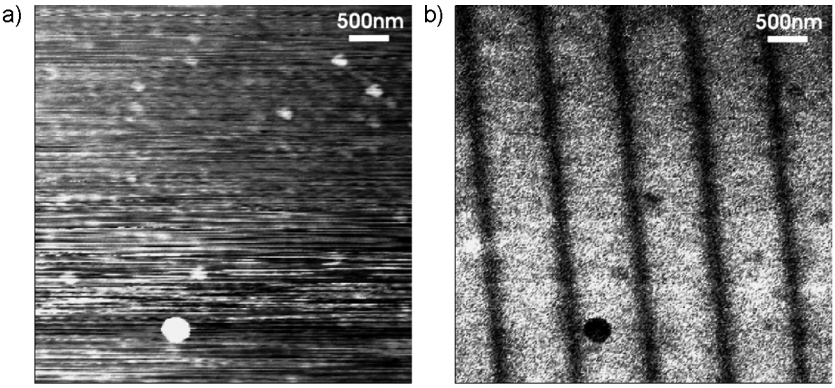

Figure 4.2: Simultaneously recorded topography and near-field fluorescent image of a fluorescence test sample acquired in contact mode. A fluorescent layer is locally bleached by means of an electron beam. The written lines are nominally 100nm wide and separated by 1μm.

in contact mode. The near-field optical image depicted in Fig. 4.2b) shows the array of lines. The simultaneously recorded topography image shown in Fig. 4.2a) displays some protruding particles on the flat sample surface.

As the topographical features are not correlated with the written lines, we can be sure that the contrast seen in the optical near-field image is a pure optical signal. However, it is important to emphasize that even a few nanometers of roughness in the sample can still lead to topography-induced optical signals. For instance, the big particle visible at the bottom of image 4.2a) has probably induced an artifact in the corresponding (Fig. 4.2b)) optical image.

As indicated in the cross section shown in Fig. 4.3 the fluorescence count rate is sufficient and the signal-to-noise ratio is good. From this image an optical lateral resolution of approximately 70nm is estimated.

An even better measure of the optical resolution is the image of individual fluorescent molecules [4].

To this purpose, a glass cover slit has been spin coated with a 10^{-8}M

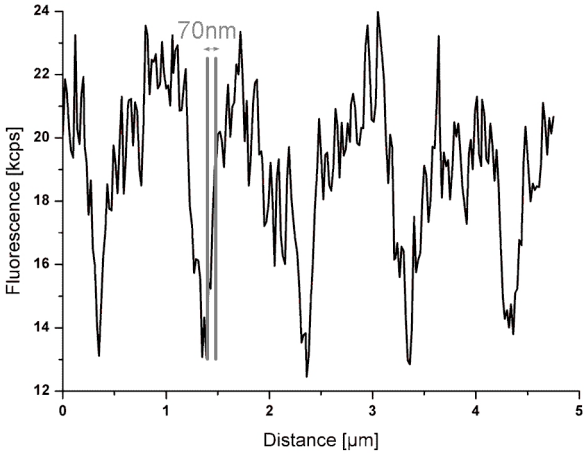

Figure 4.3: Cross section through the fluorescence image 4.2b) taken along the white line. From this cross section the resolution obtainable with the probes can be estimated to 70nm.

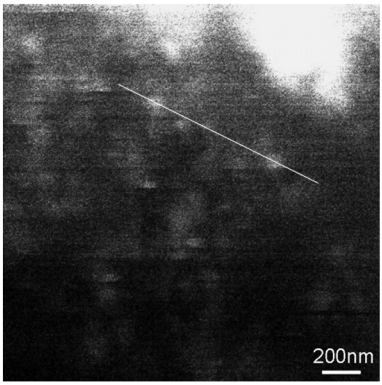

Figure 4.4: Near-field fluorescence image of fluorescently labelled molecules acquired in contact mode.

diluted solution of succinimidyl esters of the Alexa Fluor 532 dyes [2]. An additional, approximately 10nm thick PMMA layer has been deposited on the sample by spin coating.

This sample is scanned in contact mode and the resulting near-field optical image is displayed in Fig. 4.4. On this image several bright spots are visible, which we attribute to individual dye molecules. The size of these fluorescence peaks is a measure of the lateral optical resolution. As shown in the cross section graph of Fig. 4.5, the peaks which were fitted by a gaussian have a full width half maximum (FWHM) of about 65nm, confirming an optical spatial resolution well below 100nm achieved with the probes.

4.1.3 Collection mode imaging

Our SNOM probes have been tested in collection mode by E. Descrovi [3]. For collection mode imaging, a self-made microscope has been used. In that case, the sample is globally illuminated using a conventional optical system (argon laser, λ=514.5nm), and the light scattered by the sample is picked up

[2] Molecular Probes, Inc., 29851 Willow Creek Road, Eugene, OR 97402

[3] Applied Optics Laboratory, Institute of Microtechnology, University of Neuchâtel

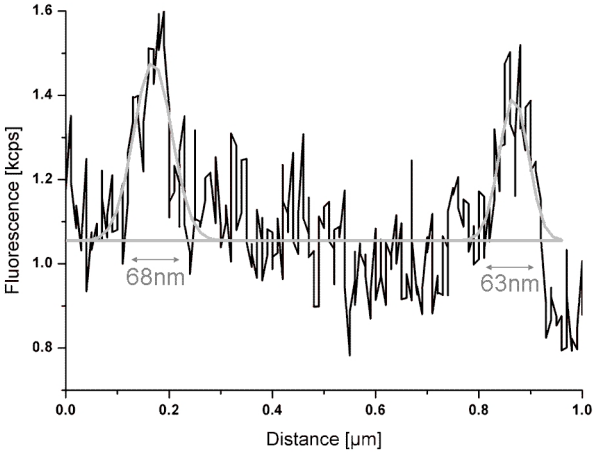

Figure 4.5: Cross section through the fluorescence image 4.4b) taken along the white line. The data is fitted by a multi-peak gaussian fit (light gray line). The optical resolution estimated by the FWHM value of the peaks is about 65nm.

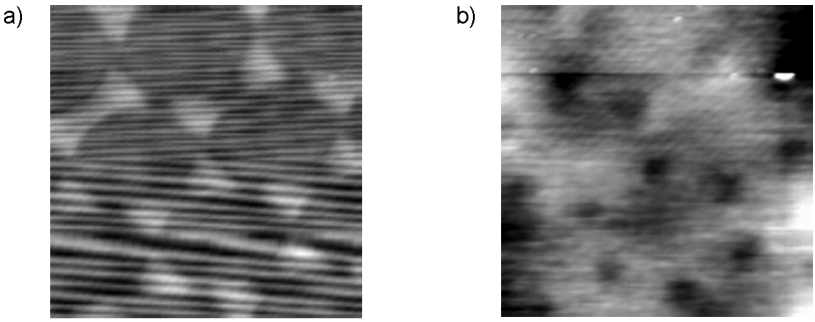

Figure 4.6: Collection mode image of a Fischer pattern. Simultaneously recorded topography (a) and near-field optical (b) image acquired in contact mode. The mean distance between two adjacent metal islands is 110nm. Image size is 1x1μm.

by means of the probe. Simultaneously acquired pictures of the topography and the transmitted near-field optical signal of a Fischer sample are depicted in Fig. 4.6. The near-field optical image (Fig. 4.6b)) looks similar to that taken in illumination mode, depicted in Fig. 4.1b). The perturbations on the topographical image are due to stray light impinging on the photodiode used for measuring the cantilever deflection.

4.2 Light coupling

The theoretical study of the electromagnetic field propagation in a fully metal coated $Si0_2$ tip presented in section 3.1 predicts that this kind of structure presents very confined emission characteristics. However, this field confinement is generated only when the radially polarized radiation mode (LP_{11}) is excited, since it is guided till the very end of the tip. The second mode (LP_{01}) leads to a light leakage at the tip flanks, when the cut-off dimensions of the waveguide are reached.

Considering the above described model, an ideal configuration for SNOM imaging with our probes, is given by the excitation of the radial polarized mode only. When both modes are excited, the high field confinement produced at the tip apex will be blurred by the light leakage at the tip flanks,

resulting from the linearly polarized mode.

In the case of an optical fiber, experiments have shown [5] that a radially polarized mode is not easy to couple into the fiber and that its polarization strongly depends on the quality of the injection. Furthermore, the far-field emission patterns depicted in Fig. 3.5 show that a certain amount of the linearly polarized light gets depolarized during propagation through the probe. Indeed, when linear polarized light is injected into the probe, the emitted light is not extinguished when a crossed analyzer is placed in front of the detector. We assume, that the light coupling or injection plays an important role in the excitation of the modes.

In order to improve the reproducibility of high resolution imaging with our probes, it is important to understand how the light injection affects their imaging capabilities, and how it is possible to control this parameter.

4.2.1 Linear input polarization

First, it has to be mentioned that for all SNOM images shown in section 4.1 a linearly polarized laser beam has been employed. This shows that high optical resolution is achievable with the fully metal coated probes even if the illumination is linearly polarized. However, only about 13% of the tested tips have shown an optical resolution below 100nm. All the tips were characterized with the scanning electron microscope before SNOM imaging, all having a tip radius of approximately 30nm.

Considering the above discussed coupling aspects, it is expected that the quality of light injection into the tip greatly affects the resulting optical resolution.

The mounting of the cantilever on the microscope head of the Alpha-SNOM is performed basically by gluing. Due to hardly controllable parameters like the amount of applied glue, the positioning of the body chip relative to the microscopy head is not very reproducible.

By imaging a Fischer sample with differently mounted SNOM chips, it could be shown that, indeed, variations of the angle of the chip relative to the microscope head, lead to small changes in the near-field optical image. The near-field optical images displayed in Fig. 4.7 show these contrast changes

due to arbitrary lateral (Fig. 4.7b)) or longitudinal (Fig. 4.7c)) tilting of a probe respective to an approximately flat mounted tip (Fig. 4.7a)).

A further parameter of the light coupling into a SNOM probe, is the focusing. The laser light can be injected into the tip for several focal point positions. We demonstrated, that the expected influence of the laser beam focusing effectively changes the achieved optical contrast. The images of Fig. 4.8 display near-field optical images of a Fischer sample taken when the input laser beam is differently focused. The hexagonal arrangement of metal island cannot be observed on Fig. 4.8a) which has been acquired while the input laser beam is focused on the $Si0_2$ back surface of the tip. But, when the focal point is lowered inside the core of the tip, some structures can be resolved with the same tip. Although this tendency could be observed for several tips, it is not repeated for every tip. On the one hand, this result supports the idea that light coupling has an influence on the field confinement at the tip apex. On the other hand, it shows also that other parameters that are hardly controllable influence the obtained near-field optical contrast.

4.2.2 Radial input polarization

Based on the theoretical calculations outlined above, by exciting the radially polarized (LP_{11}) mode propagating in the tip, the signal-to-noise ratio of the near-field optical image should increase. For that purpose, coupling of radial polarization into the tip seems to be the best way.

A radially polarized beam can be generated experimentally in several ways, for instance inside the resonator of a laser [6, 7] or by using external optical elements [8, 9]. It has to be emphasized that in the case of radial polarization the field in the focal point has a strong longitudinally oriented component in the central spot, surrounded by a ring transversally polarized. The intensity of the central spot is proportional to the numerical aperture of the focusing lens [10]. For the azimuthal polarization however, the amplitude pattern in the focal plane displays only the transversally polarized ring. In this work, this field distribution has been generated by means of a polarization converter according to that described by Quabis *et al.* [11]. It consists

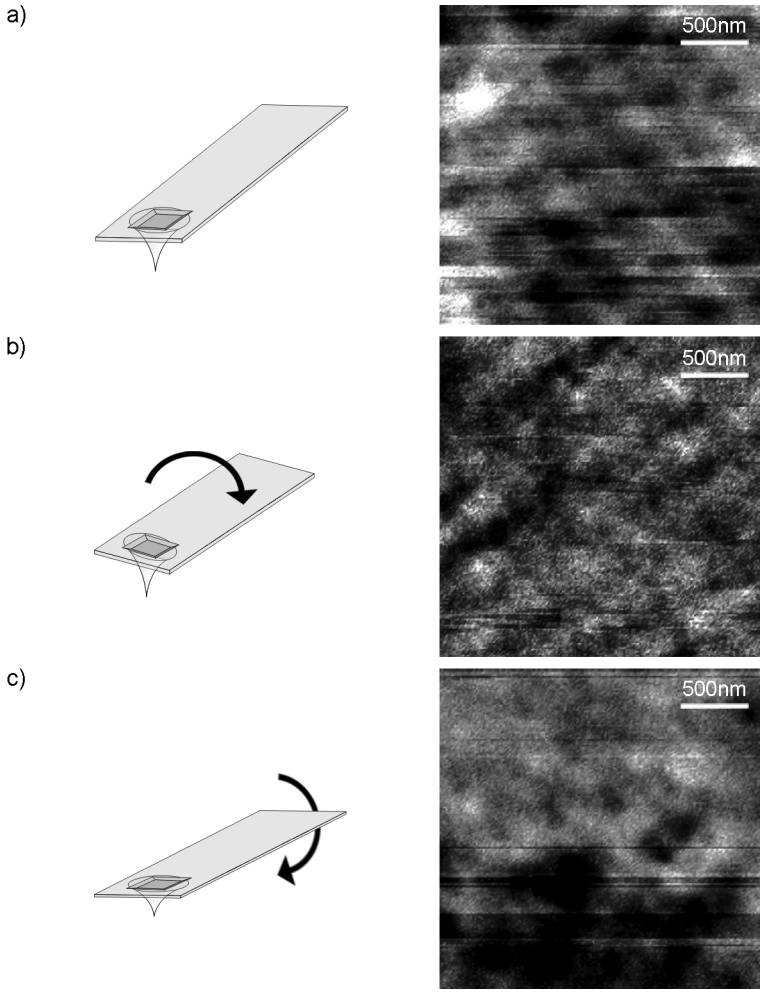

Figure 4.7: Near-field optical images of a Fischer sample acquired in contact mode. a) The probe is mounted on the microscope head by gluing. b) The probe has been tilted laterally respective to the tip used in (a). c) The probe has been tilted longitudinally respective to the tip used in (a).

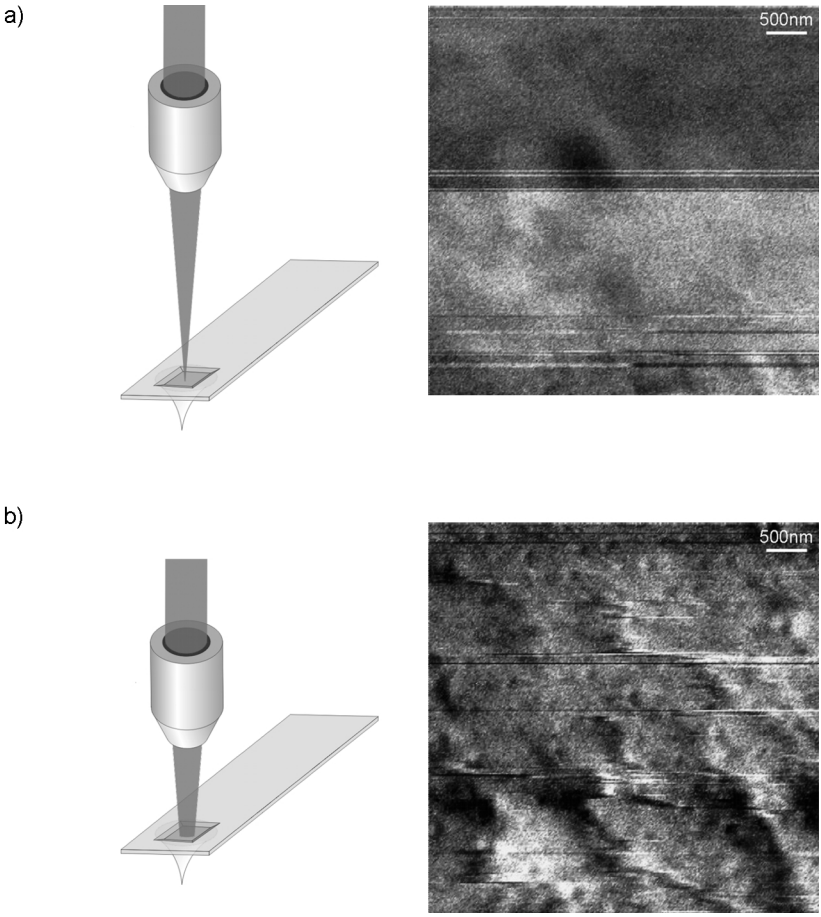

Figure 4.8: Near-field optical images of a Fischer sample acquired in contact mode. a) The input laser beam is focused on the back surface of the $Si0_2$ tip. b) The input laser beam is focused inside the tip.

of four halfwave plates that form four segments of a disk where each main axis is oriented such that the polarization of the input beam is rotated to a radial direction within each section.

The linear polarized laser beam of the AlphaSNOM passes through the polarization converter before focusing into the tip. Very distinct behaviors are observed as function of the characteristics of the tip metal coating. For tips coated in the *standard* way [4] the far-field patterns depicted in Fig. 3.5 are reproduced. For the tips presenting a much rougher metal surface [5], however, a very distinct far-field emission pattern is observed. The pictures of Fig. 4.9 display these emission patterns with and without an analyzer placed in front of the detector, which are characteristic of a radial or azimuthal polarized light beam respectively. It has to be noticed that the achievement of this far-field pattern, is extremely sensitive to the light coupling conditions.

Nevertheless, no increase of the optical resolution could be obtained in near-field optical imaging. One possible explanation of this result, is that in spite of a far-field emission pattern indicating the coupling to the radially polarized mode LP_{11}, the other mode LP_{01} is also excited. Similar to the situation with linearly polarized input light, this last mode then blurs the high optical resolution contrast.

This interpretation is supported by the work of E. Descrovi. He investigated the inverse problem of the coupling and transmission of light into the probes [12]. For that purpose, the probes were mounted in a self-made collection mode SNOM. He imaged with this instrument the focal region of an objective when either azimuthally or radially polarized light was passed through the lens. These specific polarizations were achieved with a liquid crystal cell [9]. These collection mode experiments reveal that both the longitudinal and transversal components of the field are coupled into the probe. But, the coupling coefficients of the transversal and longitudinal components of the field are dependent on the tips physical parameters. A *standard* tip couples the transversal components more efficiently, whereas a tip with the

[4] 5nm titanium adhesion layer followed by 100nm aluminum deposited in "planetary mode", see Fig. 3.9a)

[5] 100nm of aluminum deposited in "normal" mode, see Fig. 3.9c)

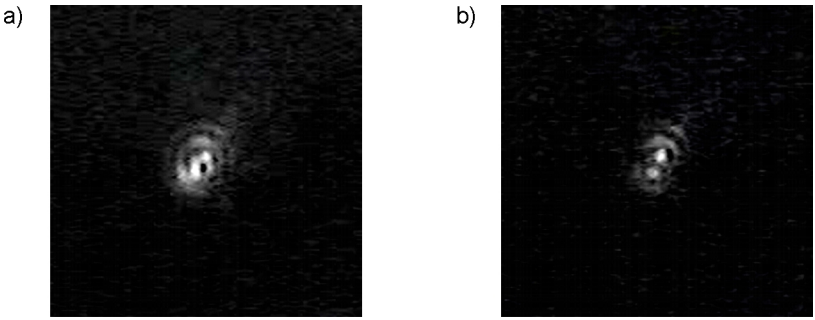

Figure 4.9: Far-field emission patterns of a fully metal coated $Si0_2$ tip for radial polarization of the illumination beam: Intensity of light transmitted through the tip without (a) and with (b) an analyzer placed between the tip and the detector. The tip is coated with 100nm aluminum in "normal" mode.

rough aluminum coating favors the longitudinal component. According to the theoretical model presented in section 3.1 it can be inferred that the transversal and longitudinal field components couple at different locations of the tip. The transverse field will more likely be coupled over a lateral region surrounding the apex, a few hundreds nanometers from it. At this location the tips dimensions allow the LP_{01} mode to be guided. For an analogous reason, a longitudinal field will be coupled at the very end of the tip. Thus, in the case of the rough tip, only the coupling of the transversal component is affected by the random assembly of aluminum grains along the tip walls. Indeed, due to huge scattering at the tip flanks, the coupling of the transversal field component is prevented. The coupling of the longitudinal component is not affected by the tip roughness, since the very apex of the tip looks similar to that of the *standard* tip.

For the illumination mode configuration, this effect of the metal coating roughness is much weaker because of the flat $Si0_2$ interface. In that case, it seems to be very difficult or even impossible to completely avoid the light leakage at the tip flanks.

4.3 Polarization aspects

Since the excitation of the only LP_{11} mode seems to be very difficult, the idea for increasing the yield of the probes is to discriminate the LP_{01} mode just before detection.

Based on the model presented in section 3.1, when a SNOM tip is brought in close proximity to the sample surface, it is expected that the emitted light will consist of light confined at the tip apex, which is polarized perpendicular to the sample surface, as well as of a background of light polarized in the plane of the sample. It should, therefore, be possible by means of a suitably placed analyzer, to block this unwanted background.

For this purpose, an analyzer was placed in front of the light detector during scanning. By changing the position of the analyzer, one can cut out the light coming from the tip flanks and therefore improve significantly the signal-to-noise ratio of the near-field optical signal [13]. A better image quality was indeed observed when the analyzer direction was perpendicular to the input polarization as shown in Fig. 4.10d), where the small metal islands of the Fischer pattern are well resolved. The near-field optical image of Fig. 4.10b), indicates that the linearly polarized mode blurs the "high resolution mode", since the structures are barely observable in this image. Working with an analyzer increases the percentage of the probes displaying high optical resolution to about 25%.

Polarization contrast mechanisms have already been applied to SNOM imaging by several authors, as for instance for illumination and collection mode SNOM [14], for reflection mode SNOM with coated [15] or uncoated [16] fiber probes, for photon scanning tunnelling microscopy [17] or even polarization-modulation SNOM [18].

It is well known that a SNOM image of a sample with dielectric or metallic surfaces displaying well defined subwavelength sized structures is, in general, very sensitive to the polarization states of the incident and detected light [14, 19, 20, 21, 22]. In the case of transmission SNOM imaging of metallic structures using polarized light, different images may be obtained depending on the orientation of the polarization [14, 23]. These differences

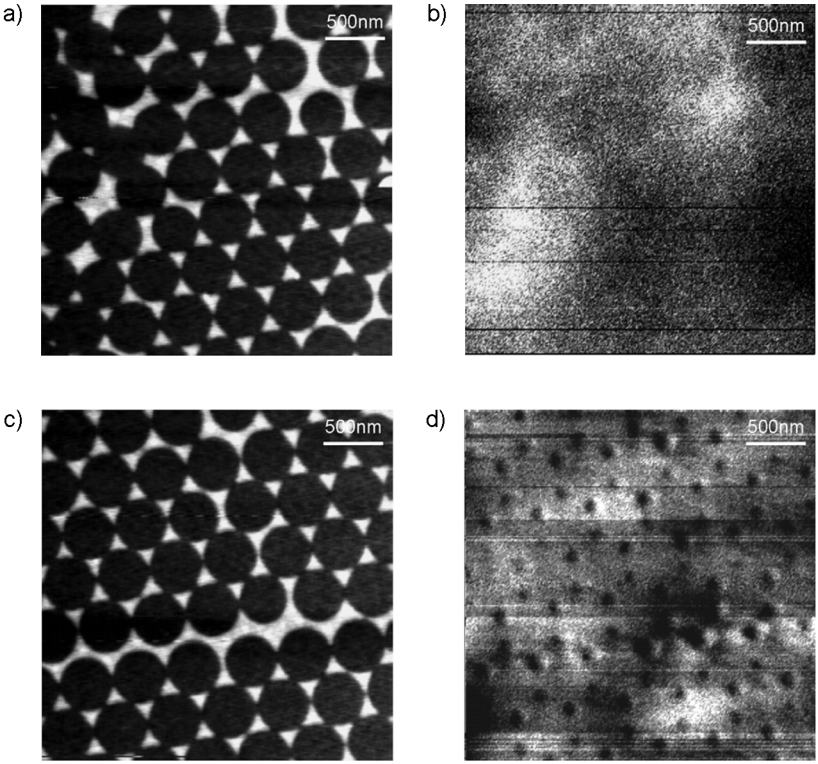

Figure 4.10: In contact mode, simultaneously acquired topography and near-field optical images of a Fischer sample, for linearly polarized illumination. (a) Topography and (b) near-field optical image of the sample without an analyzer, respectively (c) topography and (d) near-field optical image with an analyzer placed in front of the light detector during scanning.

are simply due to matching of electromagnetic boundary conditions at an interface.

The existence of these effects generated by polarization in SNOM provides, on the one hand, unique sample information, but on the other hand, complicates the interpretation of the image. Thus, when interpreting the resulting near-field images of the metallic structures of the Fischer pattern, polarization effects of both the sample and the tip, as well as the resulting probe-sample interaction must be taken into consideration.

Nevertheless, by varying the linear polarization direction of the injected light, no dramatic change in optical contrast is observed when imaging a Fischer pattern. However, it is evident that the light propagation properties and the emission of the probe itself must also be taken into account when interpreting the above near-field data. The thickness and quality of the metal coating are obviously parameters that influence the observed optical behavior of the probes (see also section 4.2.2). In particular, the excitation of the LP_{11} mode is related to different coupling parameters and also clearly to geometrical parameters like the metal coating structure.

All these results show that the emission characteristics of the SNOM probes and the resulting image interpretation are complex and, to improve their comprehension, models that take into account the different influencing parameters are necessary. Then, a careful comparison between experiments and calculations will provide a more refined understanding of the optical behavior of the probes and thus, open the door to probe optimizing in view of a better yield.

4.4 Summary and conclusions

In order to assess the optical resolution achievable with the completely metallized SNOM probes, imaging experiments on several samples have been presented. Neighboring metal islands of a Fischer sample which are 110nm apart could be well resolved. As the scans have been acquired in contact mode, topography artifacts cannot be excluded. In order to avoid these kinds of artifacts, further imaging on fluorescence test samples has

been undertaken. Moreover, fluorescence measurements are very interesting to test the sensitivity of the probes.

In section 2.7 a method for producing a fluorescence test sample that possesses high optical contrast with uncorrelated topography variation has been described. By imaging such a sample in contact mode, an optical resolution of 70nm could be shown. This result is in accordance with the imaging experiments performed on single molecule samples, for which a similar resolution could be deduced.

As only approximately 13% of the tested probes showed high optical resolution, different investigations of potentially influencing parameters have been performed. Particular attention has been paid to polarization aspects and to the light coupling into the probes.

The theoretical study presented in section 3.1 shows that high field confinement is generated at the tip apex by exciting the radially polarized radiation mode (LP_{11}) and thus suggests that high optical resolution should be achieved when this single mode is excited. Since this case seems to be experimentally extremely difficult or even impossible to realize, another method for increasing the resolution of the probes has been studied.

Considering once again the previously discussed theoretical model, the detected signal is a superposition of two polarization states, one from the tip apex and one from the light leaking out at the tip walls. Thus, the near-field optical image contrast should be increased by using an analyzer for selectively detecting light emitted from the SNOM tip apex. Experimentally, high optical resolution is observed when the linear polarized light coming from the tip flanks is discriminated during scanning. We conclude that upon coupling the light into the tip, the high resolution radial mode is excited. This mode then provides the high resolution SNOM images.

In this case, a higher percentage, about 25%, of the probes showed high optical resolution.

It has to be emphasized that the polarization behavior of the probes is probably affected by the shape of the tip and the grain structure of the metal coating. This last parameter is clearly difficult to control.

The results presented in this chapter demonstrate that polarization effects play an important role in near-field image formation, but also compli-

cate the understanding of the physical mechanism of light transmission and emission of the probes.

Few reports on fully metal coated probes have been found. Nakajima *et al.* [24, 25] introduced a hybrid system of SNOM combined with a scanning tunneling microscope (STM). Based on a similar idea, the entirely metal-coated tetrahedral tip developed by Koglin *et al.* [26] has achieved very high optical resolution. Theoretical work has also shown that a tip displaying a metal coating of reduced thickness instead of a physical hole at the tip apex, provides a much smaller near-field spot than those obtained by conventional aperture SNOM probes [27]. No direct comparison with our probe is possible since in all above mentioned approaches the metal coating at the tip apex is semi-transparent. A more similar probe has been proposed by Yatsui *et al.* [28], an entirely aluminum coated pyramidal silicon probe. In that case, the high optical throughput (2.3%) observed is attributed to localized surface plasmon resonance. High optical resolution of about 50nm is assumed.

These observations combined with our results show the great potential of entirely metal coated probes for SNOM imaging.

Bibliography

[1] U. C. Fischer, H. P. Zingsheim. *Submicroscopic pattern replication with visible light*. J. Vac. Sci. Technol. **19**, 881 (1981).

[2] B. Hecht, H. Bielefeldt, Y. Inouye, D. W. Pohl, L. Novotny. *Facts and artifacts in near-field optical microscopy*. J. Appl. Phys. **81**, 2492 (1997).

[3] P. G. Gucciardi, M. Colocci. *Different contrast mechanisms induced by topography artifacts in near-field optical microscopy*. Appl. Phys. Lett. **79**, 1543 (2001).

[4] E. Betzig, R. J. Chichester. *Single molecules observed by near-field scanning optical microscopy*. Science **262**, 1422 (1993).

[5] A. Bouhelier, J. Renger, M. R. Beversluis, L. Novotny. *Plasmon coupled tip-enhanced near-field microscopy*. J. Microscopy **210**, 220 (2003).

[6] D. W. Pohl. *Operation of a ruby laser in the purely transverse electric mode TE01*. Appl. Phys. Lett. **20**, 266 (1972).

[7] R. Oron, S. Blit, N. Davidson, A. A. Friesem, Z. Bomzon, E. Hasman. *The formation of laser beams with pure azimuthal or radial polarization*. Appl. Phys. Lett. **77**, 3322 (2000).

[8] Z. Bomzon, G. Biener, V. Kleiner, E. Hasman. *Radially and azimuthally polarized beams generated by space-variant dielectric subwavelength gratings*. Opt. Lett. **27**, 285 (2002).

[9] M. Stalder, M. Schadt. *Linearly polarized light with axial symmetry generated by liquid-crystal polarization converters*. Opt. Lett. **21**, 1948 (1996).

[10] M. A. Lieb, A. J. Meixner. *A high numerical aperture parabolic mirror as imaging device for confocal microscopy*. Opt. Express **8**, 458 (2001).

[11] S. Quabis, R. Dorn, O. Glöckl, M. Reichle, M. Eberler. *Reduction of the spot size by using a radially polarized laser beam*. Proc. of SPIE Int. Soc. Opt. Eng. **4429**, 105 (2001).

[12] E. Descrovi, L. Vaccaro, W. Nakagawa, H.-P. Herzig, L. Aeschimann, U. Staufer. *Collection of transverse and longitudinal fields by means of apertureless nano-probes with different metal coating characteristics*. to be published (2004).

[13] L. Aeschimann, L. Vaccaro, T. Akiyama, U. Staufer, N. F. De Rooij, R. Eckert, H. Heinzelmann. *Polarization properties of fully metal coated scanning near-field optical microscopy probes*. AIP Conf. Proc. **696**, 906 (2003).

[14] E. Betzig, J. K. Trautman, J. S. Weiner, T. D. Harris, R. Wolfe. *Polarization contrast in near-field scanning optical microscopy*. Appl. Opt. **31**, 4563 (1992).

[15] C. Durkan, I. V. Shvets. *Polarization effects in reflection-mode scanning near-field optical microscopy*. J. Appl. Phys. **83**, 1837 (1998).

[16] C. Adelmann, J. Hetzler, G. Scheiber, T. Schimmel, M. Wegener, H. B. Weber, H. v. Löhneysen. *Experiments on the depolarization near-field scanning optical microscope*. Appl. Phys. Lett. **74**, 179 (1999).

[17] K. Propstra, N. F. Van Hulst. *Polarization contrast in photon scanning tunnelling microscopy combined with atomic force microscopy*. J. Microscopy **180**, 165 (1995).

[18] T. Lacoste, T. Huser, R. Prioli, H. Heinzelmann. *Contrast enhancement using polarization-modulation scanning near-field optical microscopy (PM-SNOM)*. Ultramicroscopy **71**, 333 (1998).

[19] E. Betzig, J. K. Trautman, T. D. Harris, J. S. Weiner, R. L. Kostelak. *Breaking the diffraction barrier: Optical microscopy on a nanometer scale*. Science **251**, 1468 (1991).

[20] O. J. F. Martin, C. Girard, A. Dereux. *Dielectric versus topographic contrast in near-field microscopy*. J. Opt. Soc. Am. A **13**, 1801 (1996).

[21] J.-C. Weber, E. Bourillot, A. Dereux, J.-P. Goudonnet, Y. Chen, C. Girard. *Observation of light confinement effects with a near-field optical microscope*. Phys. Rev. Lett. **77**, 5332 (1996).

[22] G. Lévêque, G. Colas des Francs, C. Girard, J. C. Weeber, C. Meier, C. Robilliard, R. Mathevet, J. Weiner. *Polarization state of the optical near field*. Phys. Rev. E **65**, 036701–1 (2002).

[23] J. K. Trautman, E. Betzig, J. S. Weiner, D. J. DiGiovanni, T. D. Harris, F. Hellman, E. M. Gyorgy. *Image contrast in near-field optics*. J. Appl. Phys. **71**, 4659 (1992).

[24] K. Nakajima, V. Jacobsen, J. Noh, T. Isoshima, M. Hara. *High resolution beyond aperture size achieved by hybrid SNOM/STM system*. RIKEN Rev. **38**, 52 (2001).

[25] K. Nakajima, V. Jacobsen, Y. Yamasaki, J. Noh, D. Fujita, M. Hara. *Hybrid scanning near-field optical/tunneling microscopy with indium-tin-oxide/Au coated optical fiber probe*. Jpn. J. Appl. Phys. **41**, 4956 (2002).

[26] J. Koglin, U. C. Fischer, H. Fuchs. *Material contrast in scanning near-field optical microscopy at 1-10nm resolution*. Phys. Rev. B **55**, 7977 (1997).

[27] L. Novotny, D. W. Pohl, B. Hecht. *Scanning near-field optical probe with ultrasmall spot size*. Opt. Lett. **20**, 970 (1995).

[28] T. Yatsui, K. Itsumi, M. Kourogi, M. Ohtsu. *Metallized pyramidal silicon probe with extremely high throughput and resolution capability for optical near-field technology*. Appl. Phys. Lett. **80**, 2257 (2002).

Chapter 5

Summary, conclusions and outlook

Scanning near-field optical microscopy (SNOM) preserves the advantages of optical microscopy, while improving its resolution beyond the diffraction barrier. The basic idea of SNOM is to probe the sample of interest with a subwavelength sized source or detector. Nevertheless, the absence of high quality, reliable and economic probes has hindered the widespread use of SNOM.

Microfabrication is very promising for manufacturing highly reproducible and potentially cheap probes. Batch fabrication of the probes potentially permits to produce them in great numbers and high homogeneity. Moreover, the integration of a SNOM tip into a silicon AFM cantilever is possible with micromachining technology. On the one hand, this allows operating the probes not only in SNOM mode, but in addition and simultaneously, also in all modes of force microscopy. On the other hand, this opens the possibility to integrate deflection sensors on the cantilever [1], e.g. in view of parallel imaging.

In this work, a microfabricated SNOM probe based on the results obtained by Schürmann *et al.* [2, 3] and Eckert *et al.* [4] has been developed. In particular, the fabrication procedure of the probe has been reconsidered and brought to industrial standards. The batch fabricated probe consists of a 11μm high $Si0_2$ tip, integrated into a silicon cantilever. An opening in

the cantilever, placed underneath the tip, allows the light to be injected or detected from the back. The entire tip is homogeneously covered with an opaque metal layer, for instance aluminum.

The most critical fabrication step is the processing of the backside hole in the cantilever. Process improvement has been achieved by using photoresist spray coating, resist exposure by means of a projection aligner and cantilever thinning in two steps. Moreover, the patterning of the backside hole can be performed simultaneously with the cantilever definition. This permits to skip one photolithography step and, thus, reduce the processing costs. The required mechanical probe specifications can be very well controlled and a high uniformity across the wafer is achieved.

According to the industrial partners of the project (NanoWord), the microfabrication process of the probe is stable enough to permit their commercialization. It has to be emphasized, that uncoated probes show also great potential for AFM imaging. The very sharp and relatively hard $Si0_2$ tip having an apex radius of few nanometers is very well suited for high resolution topography imaging.

In spite of the 60nm thick aluminum layer covering the full tip, surprisingly high optical transmission through the probes is measured. The optical resolution in illumination-mode SNOM-imaging, performed in contact mode on various samples - Fischer pattern, fluorescence test sample and single molecule sample - was far better than 100nm. A comparable resolution was demonstrated by others [1] in collection mode imaging.

However, the repeatability of these results turned out to be low even with probes fabricated in a highly reproducible way. In particular, only a certain percentage (about 13%) of the probes have shown high optical resolution. In spite of being able to well control those which I think are important geometrical probe parameters (tip height and tip radius, metal coating thickness, cantilever and hole dimensions), repeatability problems similar to those of commonly used SNOM probes are encountered. This problem was

[1] E. Descrovi, Applied Optics Laboratory, Institute of Microtechnology, University of Neuchâtel

addressed together with experimental work and theoretical calculations in order to develop an understanding of the mechanism of light transmittance and emission of the probe. The goal of these experiments was also to assess the role of the different parameters that influence the light propagation and emission characteristics of the probe.

Finite element simulations of the electromagnetic field propagation and emission of the probes has been carried out by using experimentally measured parameters. Very pronounced emission characteristics are shown, when different polarized modes are considered. The coupling of the linearly polarized mode LP_{01} leads to light leakage at the tip flanks. The radial polarized mode obtained by the superposition of two orthogonal LP_{11} modes induces a subwavelength field confinement at the tip apex, as the electric field has a strong component along the probe axis. In the far-field of the probe, the input polarization state is recovered in both cases. Further, the field confinement at the tip apex strongly depends on the volume of its very apex. Moreover, the calculated light transmission is higher for tips displaying a smaller cone angle.

The measured transmittance through a tip fully coated with a 60nm thick aluminum film is in the order of 10^{-3} to 10^{-4}, which is roughly one to two orders of magnitude higher than for commonly used fiber based probes. Transmittance measurements of tips coated with different metals show the same tendency as the skin depth values of these metals, meaning that a metal with a smaller skin depth leads to smaller transmittance. Furthermore, higher transmittances are demonstrated with tips displaying a smaller cone opening angle as predicted by the model calculation. This trend was observed for all tested metal coatings.

In order to investigate if the measured high optical transmittance is due to plasmon excitations in the metal coating, spectroscopic studies were performed. No plasmon resonances in the metal coating, neither on a flat surface nor on the tip could be observed. Field enhancement at the tip is more likely caused by lightning rod effects, similar to those encountered in the apertureless SNOM configuration.

The tip temperature during illumination was measured in order to investigate eventual heating effects on the metal coating. Even for high laser input power, the tip temperature remained low. Transmission electron microscope (TEM) imaging before and after tip illumination demonstrated that no change in the granular structure of the aluminum coating occurred during illumination.

Further TEM imaging of differently metallized tips, revealed the fine structure of the metal film. Very smooth coatings with well arranged metallic grains can be obtained as well as rough coatings with randomly oriented grains.

Polarization dependent experiments showed very characteristic emission properties of the tips. When coupling linearly polarized laser light into a tip, distinct far-field emission patterns could be observed when polarizers positioned before the cantilever entrance and after the tip apex are either parallel or crossed by 90 degrees. When performing SNOM imaging with crossed polarizers, an increase of the optical contrast could be demonstrated.

The injection of radially polarized light led in most cases to the same far-field emission patterns as for linear polarized input light. Far-field patterns indicating an emission of radially polarized light could also be observed for a very rough tip coating. These emission patterns were very sensitive to the light coupling conditions. Descrovi *et al.* [5] considered the inverse situation, for which azimuthally or radially polarized light was detected by means of the probe. These experiments revealed that both the longitudinal and transversal components of the field are coupled into the probe. But, the coupling coefficients of the transversal and longitudinal components of the field depend on the metal coating of the tip. A smooth coating permits both field components to be coupled whereas a rough metal surface favors the coupling of the longitudinal field component.

It was also demonstrated that the light coupling conditions can greatly influence the optical contrast obtained in illumination mode SNOM imaging. The angle of incidence of the laser beam onto the cantilever backside or the focal point position of the beam showed variations in the resulting near-field optical images.

In spite of providing quantitative transmittance values that are several orders of magnitudes smaller than the measurements, the above described simulations show different similarities with the experiments. First, the tendency of having a higher transmittance for sharper tips is confirmed. Second, in both cases, very pronounced emission characteristics are observed depending on the polarization state of the light. For these reasons, I assume that the two experimentally observed polarization states can be understood in terms of the LP_{01} and LP_{11} modes propagating through the tip.

Thus, I conclude that upon light coupling into the probe two modes, which are characterized by different polarization states, are excited and propagate in the tip structure. The radially polarized mode gives rise to high field confinement in the near-field of the tip apex, potentially leading to high near-field optical resolution. In this case, the field gets a strong component along the tip axis which permits the mode to be guided until the very apex of the tip. In the far-field four lobes are obtained. Experimentally, this is due to the preferential directions introduced by the two polarizers. If the polarizers are simultaneously rotated, the pattern is rotated in the same way. It has to be noticed that in the theoretical results, a four lobe symmetry is also obtained in the far-field when coupling the LP_{11} modes into the tip. In that case, this is due to the preferential directions introduced artificially by the square mesh used for the FEM calculations. In an ideal case, we assume that the far-field pattern would display a doughnut shaped ring. The second propagating mode, which is characterized by a linear polarization, undergoes a cutoff when the tips dimensions become too small resulting in light emission on the tip flanks, several hundreds of nanometers above the apex. The emitted far-field pattern resembles an Airy disc. Again, a similar pattern has been obtained with the simulations. Thus, the emitted signal is a superposition between two different polarization states, one originating from the tip flanks and one from the tip apex.

Experimentally it was not possible to inject the light in such a way that only the radial polarized mode is excited. Both modes are always excited and in the most cases the linear polarized light component gives a transmittance which is five to ten times higher than that of the radial polarized light. Thus, I conclude that during SNOM imaging, high optical resolution is

achieved thanks to the radially polarized mode, but the obtained near-field optical contrast is blurred by the linearly polarized background light. In some cases it is, hence, possible to improve the signal-to-noise ratio of the optical signal by placing a polarizer in front of the detector and, thus, blocking unwanted light during imaging.

Furthermore, I conclude from various experiments, that the coupling to one or the other mode, and thus the tip performance, depends on a large number of different parameters. For instance, in the case of collection mode imaging, the metal grain arrangement of the coating is responsible for the difference in the coupling coefficient of the modes. Similarly, for illumination mode imaging, only few tips meet the conditions for preferentially coupling to the radial mode and near-field optical images with enough contrast are obtained.

Based on this model, several improved probe designs are thought up in order to optimize the coupling to the radially polarized mode or to get rid of the linearly polarized background light. For instance, a double tapered probe (Fig. 5.1a)) could permit to decrease the density of background light, by forcing it to leak out of the cone far above the tip apex. In analogy to the collection mode experiment described above, also the introduction of local roughness of the $Si0_2$ tip (Fig. 5.1b)) could scatter the linearly polarized mode far above the tip apex and thus, diminish the unwanted background in SNOM imaging. Moreover, by introducing an asymmetry in the taper region of the tip [6, 7] (Fig. 5.1c)), a preferential coupling to the radially polarized mode could be achieved. Based on the similarities of our probes with the aperture less probe concept, a "finite probe" (Fig. 5.1d)) similar to that described by Krug *et al.* [8] could be considered. In this case, the idea is again to couple more efficiently to the radially polarized mode.

Advantages of the *apertureless SNOM probe for transmission mode operation* over standard aperture probes are the higher achieved topographical resolution and the possibility to batch fabricate the probes in a reproducible way. Further, working with very small apertures (<50nm) is often impossible since the transmission becomes too low. This can't be overcome by

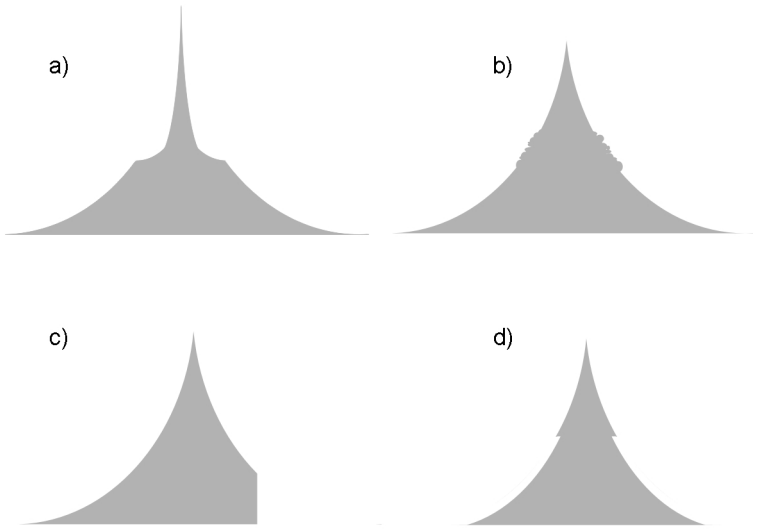

Figure 5.1: Schematics of various designs of apertureless SNOM probes for transmission mode operation in view of probe optimization: a) double tapered probe, b) probe with local increased surface roughness, c) asymmetric probe and d) semi-infinite probe

increasing the input power because of probe damage problems due to huge temperature increase. It has also to be emphasized, that an aperture probe often has a large tip apex, which strongly limits the imaging of the topography. In spite of the metal coating covering our probes, their tip radius remains small, about 30nm, providing high topographical resolution. Additionally, as our probes are entirely coated with metal, measurements involving both electrons and photos, such as combined SNOM and STM [9, 10] or biological applications like light induced ion channel current measurement are conceivable. The few reports found on entirely metal coated SNOM tips [11, 12, 9] also show the huge potential of that kind of probe.

Bibliography

[1] P. Grabiec, J. Radojewski, M. Zaborowski, K. Domanski, T. Schenkel, I. W. Rangelow. *Batch fabricated scanning near field optical microscope/atomic force microscopy microprobe integrated with piezoresistive cantilever beam with highly reproducible focused ion beam micromachined aperture*. J. Vac. Sci. Technol. B **22**, 16 (2004).

[2] G. Schürmann. *Microfabrication of combined Scanning Near-field Optical and Scanning Force Microscopy probes*. PhD thesis, University of Neuchâtel, Institute of Microtechnology, Switzerland, (2000).

[3] G. Schürmann, W. Noell, U. Staufer, N. F. de Rooij, R. Eckert, J. M. Freyland, H. Heinzelmann. *Fabrication and characterization of a silicon cantilever probe with an integrated quartz-glass (fused-silica) tip for scanning near-field optical microscopy*. Appl. Optics **40**, 5040 (2001).

[4] R. Eckert, J. M. Freyland, H. Gersen, H. Heinzelmann, G. Schürmann, W. Noell, U. Staufer, N. F. de Rooij. *Near-field fluorescence imaging with 32nm resolution based on microfabricated cantilevered probes*. Appl. Phys. Lett. **77**, 3695 (2000).

[5] E. Descrovi, L. Vaccaro, W. Nakagawa, H.-P. Herzig, L. Aeschimann, U. Staufer. *Collection of transverse and longitudinal fields by means of apertureless nano-probes with different metal coating characteristics*. to be published (2004).

[6] T. Yatsui, M. Kourogi, M. Ohtsu. *Highly efficient excitation of optical near-field on an apertured fiber probe with an asymmetric structure*. Appl. Phys. Lett. **71**, 1756 (1997).

[7] Y. C. Martin, H. F. Hamann, H. K. Wickramasinghe. *Strength of the electric field in apertureless near-field optical microscopy*. J. Appl. Phys. **89**, 5774 (2001).

[8] J. T. Krug II, E. J. Sánchez, X. S. Xie. *Design of near-field optical probes with optimal field enhancement by finite difference time domain electromagnetic simulation*. J. Chem. Phys. **116**, 10895 (2002).

[9] K. Nakajima, V. Jacobsen, J. Noh, T. Isoshima, M. Hara. *High resolution beyond aperture size achieved by hybrid SNOM/STM system*. RIKEN Rev. **38**, 52 (2001).

[10] K. Nakajima, V. Jacobsen, Y. Yamasaki, J. Noh, D. Fujita, M. Hara. *Hybrid scanning near-field optical/tunneling microscopy with indium-tin-oxide/Au coated optical fiber probe*. Jpn. J. Appl. Phys. **41**, 4956 (2002).

[11] L. Novotny, D. W. Pohl, B. Hecht. *Scanning near-field optical probe with ultrasmall spot size*. Opt. Lett. **20**, 970 (1995).

[12] J. Koglin, U. C. Fischer, H. Fuchs. *Material contrast in scanning near-field optical microscopy at 1-10nm resolution*. Phys. Rev. B **55**, 7977 (1997).

Acknowledgments

Many people have contributed in different ways to this work. Therefore, I would like to thank all those who helped me during these last few years.

First of all I deeply thank Prof. Urs Staufer, my thesis advisor. He not only supervised, guided and helped me throughout my thesis, but also was a great pedagogue in learning me the art of presentations. His encouragements, his sense of humor, his great knowledge in Physics, his always great and sometimes foolish ideas and the unforgettable USA lab tour in summer 2002, are few reasons why my time spent in his group was excellent. My special thanks go to Prof. Nico de Rooij for giving me the opportunity to do this very interesting and motivating work in his research group. It was a real pleasure to spent my thesis time in this extremely stimulating and multidisciplinary working environment. I am also very grateful to Gregor Schürmann. Without his precursor work, this thesis couldn't have been possible.

Terunobu Akiyama helped me for the design of the probes and introduced me to the "insider tricks" used in microfabrication. I highly appreciated his precious advices. Many thanks Teru! At the very beginning of the project, Wilfried Noell introduced me to the IMT clean room as well as to optical set-ups. Thank you for your help! I would also like to acknowledge the other members of the "nanotools" team: Kaspar Suter ("poussin"), Anpan Han (a little question?), Raphaël Imer (remember the nepalese meal in Amsterdam?), Sebastian Gautsch (see below), Daniel Parrat (the new Martian), Maurizio Gullo (see below), Thomas Hug, Pierre-André Künzi (see below), Ben Chui and Peter Vettiger.

Thanks to Harry Heinzelmann (CSEM), the leader of the projet, and Rolf Eckert (CSEM) for stimulating discussions and help in the optics lab.

I am also very grateful to the other industrial partners involved in the project: Thanks to Olaf Hollricher, Anita Jauss, Joachim Koenen and Klaus Weishaupt from Witec GmbH. I highly appreciated the close collaboration with Manfred Detterbeck (the big boss), Stefan Lutter (thanks for your precious help with your great knowledge in microfabrication) and Mathieu Burri (thanks for the time spent on my wafers) from Nanoworld SA. Their great technological support permitted to achieve the high quality of the SNOM probes.

The theoretical calculations presented in this manuscript wouldn't have been possible without the work of Luciana Vaccaro (Optics group, IMT). Thank you Luciana for the intense discussions, your motivation, efforts in this project and your friendship. Emiliano Descrovi (Optics group, IMT) has realized the very nice collection mode experiments. He helped me a lot for the spectroscopic measurements (...and for spending some good time in "Das schwarze Schaf"). He was also a close listener to professional and non-professional problems (MSN and Emi-icons). Thank you Emi for your support and much more!

I also would like to deeply thank Prof. Fredy Meixner (Siegen, D) and Prof. Olivier Martin (EPFL) for accepting to be co-examiners of this thesis and for their time spent in reading and correcting my manuscript. I am also grateful to Fredy for having welcomed us to his lab for performing spectroscopic measurements. Thanks also to Herbert Kneppe for his precious help in the lab. I also want to thank Olivier for the always constructive and motivating discussions.

Many thanks to Laurent Thiery (CREST, Belfort) who helped me measuring the temperature of the probes. My stay in Belfort was very pleasant and productive, ou bien...

Many thanks to Mireille Leboeuf and Massoud Dadras for their precious help in electron microscopy and sample preparation. Thank you Massoud for the hours spent at the TEM and for learning me to always put scale bars on my images (...et merci aussi d'avoir remis certaines personnes a leur place). Thanks also to both for your sense of humor, your sympathy and the

"bûche de Noël"!

Thanks also to the highly skilled technical staff of the COMLAB, without whom the hours spent in the clean room wouldn't have been the same: Sylvain Jeanneret (hockey sparring partner), Pierre-André Clerc (remember Mr Bean?), Pierre-André Künzi (the only one at SAMLAB who has a complete set of tools), Edith Millotte the fairy of the clean room (many thanks for your good advice about technical and non technical-problems), Gianni Mondin (with whom it was always a pleasure to share the women changing-room), Nicole Hegelbach (rapid, excellent work always with a smile), Sylvianne Pochon, Sabina Jenny, José Vaquera (need some help, call 5878!).

My gratitude also goes to Francine Meller for the time given to read and polish up the English of this manuscript.

I acknowledge the Board of the Swiss Federal Institutes of Technology for financial support through the program TOPNANO21.

I would like to thank the persons with whom I shared my office the most of my thesis time: Thomas Overstolz with whom I experienced a real F1 race in Ungary. Our trip to Vienna and Budapest will stay in my mind forever. Giovanni Bergonzi (mais quel beau bébé!) who entertained us every day. His jokes, amazing phone calls and sense of humor made the days in the office bright even on rainy days. Thanks also to Winston Sun ("Can I speak to Winston please?"), for his good mood and his funny stories about loosing his bike.

I am specially grateful to Sebastian Gautsch who was a steady support for technical and non-technical problems. He was an excellent student in learning the art of crosswords and always knew how to give me my smile back on bad days. My special thanks also go to Alexandra Homsy (Miss Crevette) with whom I spent the most of my time during my studies in EPFL. We shared a lot of good moments in the lab and especially outside. Thank you for your friendship, your humor and your generosity. I also shared a lot of fun with Gian-Luca Lettieri (Gian-Bond, the most sexy double of George) and Vincent Auger (your laugh was a loud sunshine at SAMLAB).

I thank my colleagues without whom the dinning breaks and sketches wouldn't have had the same flavor. Thanks to Giovanni Egidi (great cube

dancer), Quyên Pham Phoung (Pham fatale), Arash Dodge ("parce que je le vaux bien").

Many thanks to Claudio Novelli, the SAMLAB hacker, who made me laugh a big part of the day with his morning joke (because I usually understood it much later). And of course, thank you Claudio for your precious support in informatics and your help for the website. Thanks also to Florence Rohrbach for her great administrative skills and her readiness to help.

Thanks also to the other members of the SAMLAB team: Milena Koudelka-Hep, Luca Berdondini (the artist), Schahrazede Mouaziz (remember Lugano?), Laurent Dellmann (my first office-mate), Sylvain Roth, Danick Briand (let's go on the ice!), Olivier Guenat, Philippe Dubois (the surfer), Patrick Weber (the flying man), Patrick Carazzetti, Andreas Kuoni (the biker), Yves Pétremand (the bermuda guy), Michael Zickar, Vincent Linder, Bart van der Schoot, Anna Maria Spehar, Peter van der Wal, Silvia Generelli, Jan Lichtenberg (the voice), Jean-Charles Fiaccabrino (the musician), Laura Ceriotti, Sander Koster ("Kiwi"), Eva L'Hostis, Sabeth Verpoorte, Fernando Herrera.

Finally, a big "thank you" to Maurizio Gullo for his patience and his irreplaceable support in the most difficult moments.

My deepest gratitude goes to my family, my brother Gilles (Gadget) and my parents (the best parents in the world) who share my fascination for sciences and always supported me during all my life.

Publications

List of publications

E. Descrovi, L. Vaccaro, W. Nakagawa, H.-P. Herzig, L. Aeschimann, U. Staufer. *Collection of transverse and longitudinal fields by means of apertureless nano-probes with different metal coating characteristics*. To be published (2004).

L. Vaccaro, L. Aeschimann, U. Staufer, H. P. Herzig, R. Dändliker. *Propagation of the electromagnetic field in fully coated near-field optical probes*. Appl. Phys. Lett. **83**, 584 (2003).

L. Aeschimann, T. Akiyama, U. Staufer, N. F. De Rooij, L. Thiery, R. Eckert, H. Heinzelmann. *Characterization and fabrication of fully metal-coated scanning near-field optical microscopy $Si0_2$ tips*. J. Microscopy **209**, 182 (2003).

Contributions to Conferences and workshops

Proceeding

L. Aeschimann, L. Vaccaro, T. Akiyama, U. Staufer, N. F. De Rooij, R. Eckert, H. Heinzelmann. *Polarization properties of fully metal coated scanning near-field optical microscopy probes*. AIP Conf. Proc. Proc. **696**, 906 (2003).

Oral presentations

L. Aeschimann, E. Descrovi, L. Vaccaro, R. Eckert, H. Heinzelmann, T. Akiyama, U. Staufer, N. F. De Rooij. *Polarization properties of fully metal coated scanning near-field optical microscopy probes*. 12th International Conference on Scanning Tunneling Microscopy/Spectroscopy and Related Techniques (STM'03) Eindhoven University of Technology, Eindhoven, the Netherlands (2003).

L. Aeschimann, T. Akiyama, U. Staufer, N. F. De Rooij, L. Thiery, R. Eckert, H. Heinzelmann. *Characterization and fabrication of fully metal-coated scanning near-field optical microscopy $Si0_2$ tips*. 7th International Conference on Near Field Optics and related techniques (NFO-7), University of Rochester, Rochester, New York, USA (2002).

Posters

L. Aeschimann, T. Akiyama, U. Staufer, N.F. de Rooij, R. Eckert, H. Heinzelmann. *Characterization of aluminum evaporation on cantilevered scanning near-field optical microscopy (SNOM) $Si0_2$ tips*. 5th CMI-ComLab revue, Ecole Polytechnique Fédérale de Lausanne, Lausanne, Switzerland (2004).

L. Aeschimann, T. Akiyama, U. Staufer, N.F. de Rooij, R. Eckert, H. Heinzelmann. *Polarization properties of fully metal coating scanning near-field optical microscopy (SNOM) $Si0_2$ tips*. 4th CMI-ComLab revue, Ecole Polytechnique Fédérale de Lausanne, Lausanne, Switzerland (2003).

L. Aeschimann, T. Akiyama, U. Staufer, N.F. de Rooij, R. Eckert, H. Heinzelmann. *Characterization and fabrication of fully metal coated scanning near-field optical microscopy (SNOM) $Si0_2$ tips*. 3rd CMI-ComLab revue, Ecole Polytechnique Fédérale de Lausanne, Lausanne, Switzerland (2002).

L. Aeschimann, L. Vaccaro, W. Noell, U. Staufer, N.F. de Rooij, R. Eckert, H. Heinzelmann. *Cantilever based scanning near-field optical microscope probes with fully aluminum coated quartz glass tip*. 5rd Twannberg Workshop on Nanoscience, Twannberg, Switzerland (2001).

L. Aeschimann, L. Vaccaro, W. Noell, U. Staufer, N.F. de Rooij, R. Eckert, H. Heinzelmann. *Cantilever based scanning near-field optical microscope probes with fully aluminum coated tips*. Workshop "Rastersondenmikroskopie in Forschung und Industrie" by Triple-O, Basel, Switzerland (2001).

L. Aeschimann, G. Schürmann, W. Noell, U. Staufer, N.F. de Rooij. *Preparation and characterization of scanning near-field optical microscope probes*. 4rd Hasliberg Workshop on Nanoscience, Hasliberg, Switzerland (2000).